

Accepted Manuscript

Evaluating Quaternary activity versus inactivity on faults and folds using geomorphological mapping and trenching: Seismic hazard implications

Domingo Carbonel, Francisco Gutiérrez, Jorge Sevil, James P. McCalpin



PII: S0169-555X(19)30164-3
DOI: <https://doi.org/10.1016/j.geomorph.2019.04.015>
Reference: GEOMOR 6743
To appear in: *Geomorphology*
Received date: 12 February 2019
Revised date: 15 April 2019
Accepted date: 15 April 2019

Please cite this article as: D. Carbonel, F. Gutiérrez, J. Sevil, et al., Evaluating Quaternary activity versus inactivity on faults and folds using geomorphological mapping and trenching: Seismic hazard implications, *Geomorphology*, <https://doi.org/10.1016/j.geomorph.2019.04.015>

This is a PDF file of an unedited manuscript that has been accepted for publication. As a service to our customers we are providing this early version of the manuscript. The manuscript will undergo copyediting, typesetting, and review of the resulting proof before it is published in its final form. Please note that during the production process errors may be discovered which could affect the content, and all legal disclaimers that apply to the journal pertain.

Evaluating Quaternary activity versus inactivity on faults and folds using geomorphological mapping and trenching: Seismic hazard implications

Domingo Carbonel (1), Francisco Gutiérrez (1*), Jorge Sevil (1), James P. McCalpin (2)

(1) Earth Sciences Department, University of Zaragoza, 50009 Zaragoza, Spain

(2) GEO-HAZ Consulting, P.O. Box 837, Crestone, Colorado 81131, USA

* Corresponding author: fgutier@unizar.es

Abstract

The incorporation of active faults in seismic hazard analyses may have a significant impact on the feasibility, design and cost of major engineering projects (e.g., nuclear facilities, dams), especially when located in the site vicinity. The regulatory definition of active versus inactive fault is generally based on whether the fault has ruptured or not after a specific chronological bound (i.e. fault recency). This work presents a methodology, mainly based on geomorphological mapping and trenching, for determining whether specific faults can be considered as active or inactive. The approach is illustrated through the analysis of several faults located in the Spanish Pyrenees (Loiti, Leyre, La Trinidad, Ruesta faults). The 29 km long Loiti Thrust was included in the Neotectonic Map of Spain as a probable neotectonic structure. Previous works, based on geomorphological investigations, incorporated the 28 km long Leyre Thrust as a significant seismic source in a probabilistic seismic hazard analysis, which challenged the seismic design of nearby large dams. The production of

detailed geomorphological strip maps along the faults allowed the recognition of specific sites where the faults are covered by Quaternary deposits. The establishment of chronosequences (pediments-terrace sequences) and the available geochronological data helped identifying the most adequate morpho-stratigraphic units for satisfactorily evaluating fault activity vs. inactivity. The excavation of trenches at the selected sites provided unambiguous information on the presence or lack of deformation in the Quaternary cover overlying the fault, and the origin of scarps (tectonic versus erosional). Trenches were also useful for collecting samples and reliably measuring the relative height of terraces overlain by thick colluvium. The evidence gathered by these methods were complemented with the numerical dating of non-deformed slope deposits covering a fault, the analysis of the longitudinal profiles of old pediment surfaces located in the proximity of a fault, the examination of a cave situated next to a fault searching for speleoseismological evidence, and regional geodetic and seismotectonic data (GPS measurements, earthquake focal mechanisms). The integration of all the data, and especially the trenches dug in non-deformed old terrace deposits (>100 ka) truncating the faults, indicates that the analysed faults can be considered inactive and that previous neotectonic postulations were based on non-valid geomorphological interpretations.

Key words

Geomorphological mapping, Trenching, Active-fault evaluation, Pyrenees

1. Introduction

The outcome of seismic hazard assessments, either probabilistic or deterministic, may determine the feasibility of major engineering projects (e.g., nuclear facilities, dams) and may have a significant impact on their design and cost (e.g., Bommer et al., 2015). Seismic hazard estimates and seismic design parameters at a particular site of interest depend on the characteristics of the seismic sources, including earthquake catalogues and fault sources. The incorporation of active faults in the seismic source model, especially when located in the vicinity of the site and when low annual probabilities are considered, may have a significant impact on the hazard results (maximum credible event, ground motion for a given return period). Consequently, it is essential (1) to recognize and properly characterize all the active faults located in the vicinity of the site; and (2) to check the validity of the criteria used to classify the proposed active faults in the region, in order to avoid hazard under- and over-estimations, respectively. Regulatory criteria used to define active (or capable) faults generally include a chronological bound for the most recent displacement (i.e., recency of fault activity). The term capable fault is frequently used to designate active faults that can cause displacement at or near the surface (IAEA, 2015). However, according to the definitions proposed by some regulatory bodies, capable faults do not necessarily produce surface deformation (e.g., U.S. Bureau of Reclamation, U.S. Nuclear Regulatory Agency). Therefore, in this work, like in most regulatory definitions, we use the term active fault for those structures that have experienced surface displacement within the time window established by the corresponding regulation. In Spain, there is no regulatory definition for active fault (e.g., CNEGP, 1999). The Division of Safety of Dams of the California Department of Water Resources defines an active fault as having ruptured within the last 35,000 years (Fraser, 2001). These regulators argue that Holocene activity (ca. 10

ka), as proposed by the International Commission on Large Dams (ICOLD, 1998, 2016) is not a sufficiently conservative criterion and that the 35 ka age limit retains the practicality of allowing the application of several geochronological methods. However, unambiguously determining whether a fault meets this type of regulatory criterion, regardless of the established age bound, may not be feasible even in situations in which there is available geochronological data on faulted Quaternary deposits.

Figure 1 illustrates multiple scenarios and their limitations combining different: (1) stratigraphic-pedologic settings (youngest surface unit is pre-Quaternary bedrock, soil profile or Quaternary deposits); (2) geomorphic (presence or absence of scarp, which could be erosional or related to surface deformation); and (3) structural (without or with fault, which may offset different units). Other alternatives can be envisioned combining those scenarios; for instance, considering the presence of Quaternary deposits overprinted by younger soil profiles. McCalpin (2009a, Fig. 9.52) presents a complementary flow chart with indeterminate and conclusive scenarios assuming that there is an active fault according to regulatory definition.

In scenarios A and B pre-Quaternary bedrock is offset by a fault, which may and may not be expressed by a scarp, respectively (Fig. 1). Both scenarios are indeterminate, since it cannot be proved that the fault has moved after the age bound established by the regulators (e.g., 35 ka). Moreover, it may not be possible to elucidate whether the scarp is related to differential erosion (fault-line scarp) or surface deformation, and in the latter case, if the latest displacement occurred after 35 ka.

In scenarios C and D there is no Quaternary cover, but a Quaternary soil profile has developed on the faulted pre-Quaternary bedrock. In C, where the base of the soil profile does not show any offset, the situation could be indeterminate if the soil

started developing before or after 35 ka. For instance, the geometrical relationships could be essentially the same if faulting occurred at 36 ka (inactive fault) or at 34 ka (active fault) and soil development started at 37 ka or 33 ka. In scenario D, in which the base of the soil profile is displaced, the fault would be indeterminate or active if the soil development started before or after 35 ka, respectively. The use of soils for determining fault activity is complex since they do not record a depositional event, but a weathering period on a relatively stable surface. The presence of a clear offset in the soil horizons in case the fault would be active depends on multiple factors including: (1) the timing of the start of soil development; (2) the rate at which soils develop, which may vary significantly depending on climate and parent material; (3) the timing of faulting with respect to the start of soil development; (4) the amount of vertical offset; and (5) post-faulting modification of the ground surface by erosion (upthrown block) and aggradation (downthrown block). This is illustrated by the Gedanken experiment shown in figure 2, which explores the final situation depending on the timing of faulting and incorporating the following assumptions: (1) soil development starts at 50 ka; (2) the rate of soil development determines the formation of A, Bw, Bt, and Cox horizons over periods of 10 kyr, 20 kyr, 30-40 kyr and 50 kyrs, respectively; (3) fault throw is approximately half of the thickness of a fully developed soil; and (4) after faulting, the footwall and its soil profile are eroded “instantaneously” to the level of the downthrown block, which may restart or set back the soil clock. The determination of fault activity on the basis of soils may require a specific analysis considering the multiple local factors indicated above.

Scenarios E, F and G show different situations with faulted Quaternary deposits (Fig. 1). E and G show throughgoing faults that reach the surface, with an associated fault

scarp in the latter case. In scenario F the fault offsets an old Quaternary unit and is truncated and buried by a non-faulted younger deposit. In E and G, the fault can be conclusively classified as active if the deformed deposit is younger than 35 ka, and indeterminate if the age is older than 35 ka; faulting could have occurred either before or after 35 ka. Scenario F offers the possibility of having two age controls. If the older faulted unit would be younger than 35 ka, the fault would be active and indeterminate if older than 35 ka. The fault would be inactive in the younger non-deformed unit would be older than 35 ka.

Scenarios H, I and J show non-faulted Quaternary deposits that may have a scarp and different morpho-stratigraphic arrangements. In case there is a concealed fault, it would be inactive if the undeformed Quaternary cover is older than 35 ka and indeterminate if younger than that age. In Scenario I the erosional scarp is related to the development of an inset strath surface (e.g., fill-strath terrace). In J there is a younger aggradational unit inset into the older one. A trench excavated across the scarp would expose a steep contact between two different age units (e.g., buried scarp, erosional channel margin) that could be misinterpreted as a fault, especially if the excavation is not deep enough to reach non-faulted bedrock. The amount of deformation in old units should be equal or larger than that identified in overlying younger units.

The different scenarios illustrate that conclusive determination of fault activity or inactivity according to the regulatory definition is dependent on (1) the presence of markers associated with the fault and with adequate age; and (2) the availability of reliable geochronological data. Inactivity is demonstrated by non-faulted markers older than the chronological bound established by the regulator and activity by faulted

markers younger than that bound. Indeterminate situations arise when the faulted and non-faulted markers are older and younger than the reference age, respectively.

Active faults may have a decisive impact on earthquake hazard for dam projects (e.g., Brune, 1993; Tosun et al., 2007), which include as main components ground shaking, surface faulting and earthquake-triggered landsliding (Wieland, 2014). For instance, the 2008 M_w 7.9 Wenchuan earthquake, China damaged 1,803 dams and reservoirs (Wieland and Chen, 2009). The 2011 M_w 9.0 Tohoku earthquake, Japan, caused the failure of an 18 m high embankment dam resulting in 8 fatalities. The worst-case scenario is the presence of active faults at the dam foundation, posing a surface-rupture hazard that may eventually compromise the integrity of the structure (ICOLD, 1998; Wieland et al., 2008). A number of dams have been directly affected by coseismic fault movement, such as the Upper Crystal Springs Dam, USA (1906 San Francisco earthquake); Shih-Kang Dam, Taiwan (M_w 7.7 1999 Chi-Chi earthquake, Taiwan); Matahina Dam, New Zealand (M 6.3 1987 Edgecumbe Fault earthquake). This situation may require (1) the abandonment of the project; (2) the relocation of the dam site (e.g., Sayano-Shushenskaya Dam and Charvak Dam, Uzbekistan); (3) the modification of the type of structure (e.g., conservative embankment dams instead of concrete dams); (4) the incorporation of a special design such as slip joints above the fault in concrete dams (e.g., Clyde Dam, New Zealand; Inguri Dam and Morris Dam, USA) or large self-healing transition zones and ductile cores in embankment dams (e.g., Coyote Dam and Cedar Springs Dam, USA; Rogun Dam, Tajikistan; Tarbela Dam, Pakistan); or (5) the reinforcement of the structure (e.g., Matahina Dam, New Zealand). The discovery of a seismogenic fault in the vicinity of a dam after or during its

construction may affect the validity of the seismic design parameters of the structure and compliance with safety requirements.

Evidence of Quaternary deformation has been reported in multiple sites of the Spanish and French Pyrenees. Lacan and Ortuño (2012) published a comprehensive review on active seismotectonics in the Pyrenees, including an inventory of Quaternary deformation. However, these authors indicate that some of the reported recent deformation, eventually used to infer regional stress regimes (e.g., Philip et al., 1992; Goula et al., 1999), are probably related to non-tectonic processes, as supported by various recent investigations, including glaciotectonics (López-Martínez, 1986), sackung (Gutiérrez-Santolalla et al., 2005, Gutiérrez et al., 2008; Ortuño, 2009; McCalpin and Corominas, 2019), landsliding (Gutiérrez et al., 2012), dissolution-induced subsidence (Gutiérrez et al., 2016; Fabregat et al., 2017) or salt flow (Lucha et al., 2012, Gutiérrez et al., 2015). Other neotectonic interpretations are based on weak indirect evidence (e.g., clustering of low-to-moderate earthquakes, assumed geomorphic correlations) or have been challenged. For instance, in the western French Pyrenees, Alasset and Meghraoui (2005) proposed that the 50 km long Lourdes Fault is an active seismogenic structure that could produce large M_w 6.5-7.1 earthquakes. They inferred from two trenches evidence for a late Holocene surface rupture and suggested that the seismic hazard in SW France should be re-assessed incorporating the Lourdes Fault in the source model. However, this interpretation was dismissed by the neotectonics and paleoseismology (NEOPAL) expert committee, indicating that the reverse fault documented in one of the trenches (Arcizac site) is related to landsliding and that the normal fault interpreted on the other trench (Capbis site) corresponds to a steep erosional contact (i.e., channel margin) (Sébier and Meyer, 2008).

In September 2004, during the first filling of the Itoiz Reservoir, western Spanish Pyrenees, a seismic series occurred in the vicinity of the dam. The main shock reached a body-wave magnitude of M_{bLg} 4.6 and was felt in the epicentral area with a maximum intensity of EMS V (Ruiz et al., 2006a). According to García-Mayordomo and Insua-Arévalo (2011), “the event generated a significant social awareness that was used by social groups aided by a few academics to put the security of the dam under question, and particularly the stability of the left abutment”. The Spanish Ministry of Environment requested the performance of a probabilistic seismic hazard analysis (PSHA) providing results in terms of strong ground motion to be used in dynamic stability analyses of the dam and the slopes of the reservoir. A complementary study on active tectonics in the surroundings of the dam was also recommended by the Ministry of Environment. As a result, Insua and García-Mayordomo (2009), on the basis of a geomorphological investigation, proposed that the 26 km long Leyre Thrust is an active seismogenic structure. This fault is located 20 km to the south of the Itoiz Dam and 2.5 km north of the Yesa Dam. The latter dam, currently in operation, is being enlarged (from 78 m to 108 m high) to approximately double the storage capacity of the reservoir. The results of the PSHA, which included the Leyre Thrust as a relevant seismic source, was presented to the Ministry of Environment (González de Vallejo et al., 2010) and was published in a scientific journal (García-Mayordomo and Insua-Arévalo, 2011). The hazard results indicated a peak ground acceleration at the dam site for the 1000-yr return period and rock-type terrain of 0.127g, significantly higher than the values estimated in 1992 for the Itoiz Dam project (0.08g) and the NCSE-02 Spanish seismic code of 2002 (0.065g).

Furthermore, a mining company, willing to exploit a potash-bearing saline formation south of the Yesa Reservoir by the room and pillar method with subsequent backfilling, recently submitted an environmental impact assessment to the Spanish Ministry of Environment. The Ministry of Environment, following the recommendation of the Spanish Geological Survey and a committee of experts, requested investigations aimed at determining whether some nearby faults (Loiti, La Trinidad, Yesa, Ruesta faults) show any evidence of Quaternary activity. The underlying justification was that the seismic design parameters derived from the Spanish seismic code would be inadequate in case there would be an active fault capable of producing large earthquakes in the region, as suggested by García-Mayordomo and Insua-Arévalo (2011). This work illustrates how geomorphological and trenching investigations can be applied to assess whether some specific faults show any evidence of Quaternary activity.

2. Geological and geomorphological setting

2.1. Stratigraphy and structure

The study area is located in the Pyrenees, an Alpine orogen related to the convergence and collision between the Euroasiatic plate and the Iberian microplate during Late Cretaceous and Tertiary times (Fig. 3). The study region forms part of the South Pyrenean Zone on the Spanish side of the Pyrenees, characterized by outcrops of post-Variscan (Mesozoic and Tertiary) sedimentary rocks affected by S-verging folds and thrusts (Barnolas and Pujalte, 2004). The investigated faults and folds are located within the Jaca-Pamplona Basin, in the western sector of the South Pyrenean Zone (Fig. 3). This is an E-W trending foreland basin incorporated into the Pyrenean orogen

by the southward piggy-back propagation of the thrust system during the development of the orogenic wedge (Teixel, 1996). The Eocene-Oligocene fill of the basin shows an overall regressive sequence, changing upwards from marine sediments with deep turbiditic facies into continental alluvial and fluvial formations (Barnolas et al., 2004).

The formations exposed in the investigated area include sediments deposited before the development of the Jaca-Pamplona Basin (Late Cretaceous-Paleocene) and units of the basin fill (Eocene-Oligocene), all of them affected by E-W- to WNW-ESE-oriented and S-verging compressional structures and younger transverse extensional faults with limited length (Fig. 3). The main stratigraphic units relevant to the present work are indicated below in ascending stratigraphic order. The Late Cretaceous – Late Eocene formations deposited before the initial configuration of the Jaca-Pamplona Basin include calcarenites and calcareous sandstones of the Marboré Sandstone Fm., siliceous sandstones and conglomerates ascribed to the Arén Sandstone Fm. (López et al., 1997), continental sediments of the so-called Garumn Facies, attributed to the Tremp Fm. (Rosell et al., 2001), and a thick unit of marine carbonate rocks with interlayered calcareous sandstones, capped by the Alveoline Limestone (López et al., 1997).

During the initial development of the Jaca-Pamplona Basin, between the Ypresian and the Lutetian (Early-Middle Eocene), the basin was characterized by an asymmetric configuration, comprising a deep trough with turbiditic sedimentation (Hecho Group) at the foot of the orogenic wedge, and carbonate platforms associated with the foreland margin (Guara Limestone Fm.) (Barnolas et al., 2004; López et al., 1997) (Fig. 3).

In the Bartonian (Late Eocene) there was a significant paleogeographic change in the basin (Puigdefábregas, 1975). A thick succession more than 2000 m thick, dominated by blue marls, was deposited atop the Guara Limestone and the Hecho Group (Montes, 2009) (Fig. 3). This includes, from base to top, the Arro-Fiscal Marls Fm. (ca. 350 m thick) and the Pamplona Marls (ca. 2000 m thick) both separated by the Sabiñanigo Sandstone and a correlative unit to the west, represented in the Sigués village area by re-sedimented calcareous breccias with nummulites and glauconite and some sandstone beds (Puigdefábregas, 1975). In the Yesa Reservoir area, the Pamplona Marls are conformably overlain through a gradational contact by a flyschoid succession 70-150 m thick of alternating marls and sandstones known as the Yesa Flysch (Puigdefábregas, 1975; López et al., 1997).

Marine sedimentation culminates in the Priabonian (Late Eocene) with the development of the so-called Navarrese Potassic Basin and the deposition of the Guendulain Fm. (Fig. 3). This is a 150-200 m thick unit that includes a saline section with the potash salts targeted by the mining project (Rosell and Pueyo, 1997). The Guendulain evaporites, or the equivalent residual material related to its interstratal karstification, are overlain by the so-called "Banded Marls", consisting of light brown marls with sandstone intercalations in the upper part with an aggregate thickness of 15-20 m. The Liédena Sandstone, 50-80 m thick, concordantly overlies the "Banded Marls". This resistant unit with prominent geomorphic expression is interpreted as shallow marine facies (Montes, 2009). The Liédena Sandstone is overlain by a thick Late Eocene-Oligocene detrital succession several kilometers thick dominated by reddish fluvial and alluvial deposits with an overall fining-upward trend corresponding to the Campodarbe Group.

The cartographic relationships and the analysis of the syn-tectonic formations in this sector of the South Pyrenean Zone indicate a southward progression of the deformation, towards the foreland (Teixell, 1996). The northernmost thrusts (Lakora, Larra) were active in Late Cretaceous and Early Eocene times. The Gavarnie Thrust, whose leading edge emerges within the Jaca-Pamplona Basin through the Leyre and Loiti thrusts, was active between the Late Eocene and the Early Oligocene. Finally, the Guarga Thrust, which crops out in the External Sierras (southern edge of the Pyrenees), was active during the Oligocene and Early Miocene.

Two main groups of structures have been recognized in the investigated area (Fig. 3): (1) Long folds and thrusts with a dominant E-W to ESE-WNW trend and S vergence, related to the Pyrenean compression, and (2) Short transverse normal faults, clearly superimposed on the previous contractional structures, mainly concentrated south of the Yesa Reservoir around the Ruesta village and the valley of the Regal River. The main thrusts, with a NE-stepping and overlapping arrangement, are the 28 km long Leyre Thrust, and the 29 km long Loiti Thrust (Puigdefábregas et al., 1976; García et al., 1994) (Fig. 3). In the overlapping zone between these two faults, SE of Lumbier village, there is another thrust around 6 km long with smaller displacement called La Trinidad Thrust. In the southern sector of the study area, the Eocene-Oligocene succession is affected by a series of ESE-WNW folds and S-verging thrusts with limited displacement including, from N to S: (1) The 50 km long Undués-Los Pintanos Synclorium (also known as San Juan de la Peña Synclorium; Montes, 2009). This is an asymmetric synformal structure on the southern margin of the Aragón River valley, with a steeper southern limb; (2) The 50 km long Magdalena Anticline, whose steeper, locally overturned southern forelimb is offset by the N-dipping Magdalena reverse fault, with

an estimated displacement lower than 100 m. The normal faults are represented by the NNE-WSW trending Ruesta Fault system. The Ruesta Fault is the longest one (<10 km) and with greater displacement (ca. 650 m).

2.2. Seismotectonics

The Pyrenees is considered a slowly deforming orogen with low to moderate seismicity. Rigo et al. (2015), based on a GPS survey with 74 stations spanning 18 years, infer a deformation field with velocities lower than 1 mm/yr across the range and estimate a maximum extensional horizontal strain rate of 2.0 ± 1.7 nanostrain per year in a N-S direction in the western part of the range. More recently, Nguyen et al. (2016) measured NNE-SSW extensional strain rates in the western Pyrenees of up to 4 nanostrain per year. These authors interpret that the collision that generated the Pyrenees has ceased and that it can be considered as an inactive plate margin. The analysis of focal mechanisms indicates lateral variation of the style of faulting, from compression and extension in the east to strike-slip and extension in the western sector (Ruiz et al., 2006b; Lacan and Ortuño, 2012; Martín et al., 2015; Rigo et al., 2015).

According to the earthquake catalogue of the Spanish National Geographic Institute, between 1373 and 1924, the Pyrenees was struck by a total of eleven historical earthquakes felt with intensity (EMS-98) equal or larger than VIII. The 1373 intensity IX Ribagorza earthquake had its epicentre in the central Pyrenees around 150 km east of the study area. The events that have caused the largest damage were the so-called 1427-1428 seismic crisis in the eastern Pyrenees (Olivera et al., 2006). The 1428 intensity IX-X event destroyed the village of Queralbs and killed around 800 people (Martínez-Solares and Mezcua, 2002). This spatial and temporal earthquake cluster is

attributed to the sequential rupture of several segments of the Amer Fault (Perea, 2009; Zarroca et al., 2012). This is a transverse extensional structure related to the development of the post-orogenic Ampurdán graben system, superimposed on the Pyrenean contractional structures. Interestingly, no primary surface ruptures have been attributed to any of the historical earthquakes. The instrumental catalogue includes five events with magnitude larger than 5.

The largest earthquake in the region is the Martes (or Berdún) event of July 10, 1923 (Martínez-Solares and Mezcuca, 2002), which is also the largest earthquake recorded instrumentally in the Pyrenees (Stich et al., 2018) (see epicentral location in Fig. 3). According to the earthquake catalog of the Instituto Geográfico Nacional (IGN), this earthquake, which did not produce any surface rupture or fatality, reached an epicentral intensity of VII. Stich et al. (2018), based on the analysis of 20 seismograms from nine European observatories, estimate for this event a magnitude of $M_w 5.4$, a centroid depth of 8 km, and a pure normal faulting source with a strike roughly parallel to the structural grain (N29E), 66N dip. They interpret that the source was a blind structure located below the basal thrust of the Pyrenees, situated at ca. 4-5 km depth (Teixell, 1998) and attribute the deformation to a post-orogenic collapse process. A comprehensive review on the seimotectonic of the Pyrenean orogen can be found in Lacan and Ortuño (2012).

2.3. Morphostructure

The main drainage of the investigated area is the Aragón River (Figs. 3, 4). This fluvial system has carved a broad E-W-oriented strike valley (Canal de Berdún) in the easily erodible Eocene marls of the footwall of the Leyre Thrust. The northern margin of this

valley is formed by the large escarpment of the Leyre Range, with a local relief of more than 900 m. This range is underlain by the resistant Cretaceous and Paleogene limestones and sandstones of the hanging-wall of the Leyre Thrust. The southern margin of the valley, with less prominent topography, is mainly controlled by cuesta scarps developed on the Liédena Sandstone and Campodarbe Group with a general S-dip. In this section of the valley, the Aragón River has developed an extensive stepped sequence of terraces and mantled pediments (Fig. 4). The Esca River and the Regal River are discordant tributary drainages that traverse the Leyre Thrust and the Ruesta Fault, respectively. Downstream of the Yesa village, the Aragón River changes into a transverse drainage sub-perpendicular to the structural grain and receives the flow of the Irati River upstream of Sangüesa town. The Irati River is the main drainage in the western sector, together with its tributary the Salazar River. These fluvial systems have excavated a broad erosional depression in Eocene marls upstream of the Lumbier Anticline, where they have developed a widespread system of terraces and mantled pediments (Fig. 4). The Irati River traverses perpendicularly the WNW-ESE-oriented Lumbier Anticline through a narrow limestone canyon (Lumbier Canyon). Downstream, the river veers into a strike-parallel ESE-WNW orientation along a relatively wide valley section associated with the Loiti Thrust and has well-developed terraces in this reach.

3. Methodology

Initially, two detailed geomorphological strip maps were produced showing the analyzed faults and the associated Quaternary landforms and deposits, mainly pediments and terraces. One of the maps covers: (1) the range and piedmont associated with the Leyre Thrust, on the northern margin of the Aragón River; (2) the

La Trinidad Thrust east of the Irati-Salazar valley; and (3) the eastern portion of the Loiti Thrust and its hanging-wall anticline (Lumbier Anticline), which are traversed by the Irati River. The other strip map covers the Ruesta Fault, at the southern margin of the Aragón valley, which is traversed by the Regal River. The following data were used for the production of the maps: (1) aerial photographs of the Instituto Geográfico Nacional (IGN) from different dates and printed at various scales (1956, 1:33,000; 1967, 1:18,000; 1997-2000, 1:20,000); (2) orthophotographs from 2012 with a spatial resolution of 0.5 m/pixel (IGN); (3) a LiDAR-derived DEM with a spatial resolution of 5m/pixel (IGN); (4) the sheets 174-II (Lumbier) and 175-I (Tiermas) of the Geological Map of Navarra at 1:25,000 scale (López and Solé, 1997a, b; López et al., 1997); and (5) various sheets of the 1:50,000 scale Geological Map of Spain (Puigdefábregas et al., 1976). After conducting thorough field surveys, the maps were produced in a GIS environment and using a vector graphics editor.

Topographic profiles were measured in the field with a range finder (Advantage Laser Atlanta) that provides azimuth, inclination, and horizontal and vertical distance values between measuring stations. Longitudinal topographic profiles of pediments located in the piedmont of the Leyre Range were constructed with the 5 m resolution DEM and using GIS tools. Trenches were excavated in terrace deposits with backhoe. The deep (10 m) and large-volume trench excavated in the Ruesta Fault required the use of two large backhoes and trucks to extract the excavated sediment, with a total cost of 57,000 euro. One of the walls of each trench was logged on graph paper after placing a grid with cord and nails with variable spacing (1-4 m), depending on the complexity of the stratigraphy and structure. Charcoal samples collected from slope deposits overlapping the Leyre Thrust were dated at Beta Analytic. The Peña Blanca Cave, located

in a difficult-access escarpment at 1.4 km distance from the trace of the Leyre Thrust was examined with the assistance of the speleologist who mapped the cave (Fig. 4).

4. The Lumbier Anticline and the Loiti Thrust

4.1. Previous work

Insua and García-Mayordomo (2009) and González de Vallejo et al. (2010) conducted a geomorphological and geochronological investigation on the terraces of the Irati River upstream and downstream of the Lumbier Anticline, which is the hanging-wall fault-propagation fold of the Loiti Thrust. These were postulated as adequate morphostratigraphic markers for identifying and assessing recent activity on the associated contractional structures. They produced a geomorphological map differentiating seven terrace levels (T0:+47 m; T1:+40 m; T2: +36 m; T3: +30 m; T4: +24 m; T5: +10 m; T6: +5 m) and two alluvium-mantled pediments, and carried out geochronological analyses. Based on their geomorphological analysis, including topographic profiles constructed with DEMs, they deduced that the Lumbier Anticline has been active during the Quaternary (growing fold). This interpretation was based on two main geomorphic anomalies:

(1) The surface of a T1 terrace of the Irati River on the northern limb of the Lumbier Anticline is situated at a relative height above the channel of at least 4 m higher than expected (+44 m instead of +40 m or +36 m) and shows an anomalous northward upstream inclination (see location of trench TIN in Fig. 5).

(2) South of the Lumbier Anticline, where the Irati Valley veers into a ENE-WSW orientation subparallel to the structure, the authors, on the basis of topographic profiles, recognized an anomalous down-valley gradient of 2° in an alluvial surface that

they attributed to their T1 terrace (see location of trenches TIS1 and TIS2 in Figs. 5 and 6). Insua and García-Mayordomo (2009) contended that, although an ESE tilting is not consistent with the growth of a WNW-ESE trending anticline, the high slope of the terrace must be related to neotectonic deformation, probably due to the interplay of secondary faults.

Insua and García-Mayordomo (2009) and González de Vallejo et al. (2010) obtained eight numerical thermoluminescence (TL) ages from samples collected in terraces (4), pediments (3) and colluvial deposits (1). A sample from the deposit of terrace T1 (+40 m) yielded an age of $108 \pm 39/-22$ ka. Their terrace level T2 (+36 m) is dated with one sample at $117 \pm 44/-24$ ka (overlapping the previous age). On the basis of these data, the authors attribute to the T1 terrace a minimum age of 108 ka. A sample collected in the apparently uplifted terrace deposit at the northern limb of the anticline yielded an age of $85.7 \pm 24.0/-15.8$ ka. This age led the authors to consider that the putative deformed terrace deposit could correspond to either T1 (+40 m) or T2 (+36 m), and consequently the vertical displacement could range between 4 m and 13 m.

Based on the inferred Quaternary activity of the Lumbier Anticline, they postulate that the Leyre Thrust, located to the NE and beyond the La Trinidad Thrust, can be considered a seismogenic source (Figs. 3, 4). The authors do not explain why they decided to categorize the Leyre Thrust as a seismogenic source and not the Loiti Thrust, which is geometrically and genetically associated with the Lumbier Anticline. For the characterization of the Leyre Thrust, Insua and García-Mayordomo (2009) and González de Vallejo et al. (2010) assume a rupture length of 26 km, a 30°N dip and a seismogenic depth of 5-6 km. Using these geometrical parameters and the empirical relationships of Wells and Coppersmith (1994) they estimate moment magnitudes of

6.53±0.25 (rupture area) and 6.73±0.28 (surface rupture length) and a mean value of M_w 6.6±0.26. With these magnitudes and using the Wells and Coppersmith (1994) relationships, they estimate mean displacement per event between 0.61 m and 0.69 m and maximum displacement per event between 1.19 m and 1.43 m. Earthquake recurrence was assessed considering that the terrace onlapping the northern limb of the Lumbier Anticline has been uplifted 8 m, involving a net displacement of 16 m on the thrust, dipping 30N. With a cumulative displacement of 16 m and ascribing an age 100 ka to the uplifted terrace, they calculate a mean slip rate for the Leyre Thrust of 0.16 mm/yr. Based on these rates and the values of displacement per event they further calculate an average recurrence of 6,124 years. Similar values are obtained using the relationships of Slemmons (1982) and Aki (1966); 5,500 and 6,631 years, respectively.

This fault characterization was incorporated into the PSHA for the Itoiz Dam site, situated 20 km north of the Leyre Thrust. The aim of the PSHA was to obtain strong ground motion parameters to be used in dynamic stability analyses for the dam and the slopes of the reservoir. The PSHA was elaborated for the Spanish Ministry of Environment (González de Vallejo et al., 2010) and published in a scientific journal (García-Mayordomo and Insua-Arévalo, 2011). The source model of the seismic hazard analysis included two types of sources: (1) Sixteen zones within a 150 km radius from the Itoiz Dam site, for which an earthquake catalogue was produced. (2) A single fault source corresponding to the Leyre Thrust, which was incorporated in the analysis following a time-independent characteristic earthquake model (Youngs and Coppersmith, 1985). The criteria used to select fault sources included evidence of activity younger than 125 ka and a distance to the site lower than 25 km. The obtained

peak ground acceleration (PGA) for rock-type terrain and the 1000- and 5000-yr RP were 0.127g and 0.300g, respectively. The 1000-yr RP value is significantly higher than those estimated for the Itoiz Dam project (0.08g) and in the NCSE-02 Spanish seismic code (0.052g). The analysis of the hazard results indicated that the main contributing sources in order of importance are the zone in which the Itoiz Dam is located and the Leyre Thrust. A deaggregation analysis revealed that the controlling earthquake for the 5000-yr return period is the maximum earthquake established for the Leyre Thrust (García-Mayordomo and Insua-Arévalo, 2011).

4.2. Evaluation of the neotectonic interpretation

A new 1:5,000 scale geomorphological map was produced that focused on the alluvial levels developed by the Irati and Salazar rivers upstream and downstream of the Lumbier Anticline, which is traversed discordantly by the Irati River through the Lumbier Canyon (water gap). A simplified version of this map is integrated in Figure 4. Five main alluvial levels were differentiated (V to I from older to younger). The two oldest ones (PV-TV and PIV-TIV) and level TII-PII are represented by terraces (T) and correlative mantled pediments (P). The rest of the alluvial levels are recorded by terraces (TIII and TI). The terraces show consistent relative heights above the river channel: TV:+47 m; TIV:+40-45 m; TIII:+35 m; TII:+20 m; TI:+2-9 m. Our TIV terrace coincides with the T1 terrace of Insua and García-Mayordomo (2009). Terrace and pediment deposits are typically less than 3 m thick, dominated by gravelly facies and overlie flat strath surfaces cut across dipping bedrock.

Initially, a N-S-oriented topographic profile was constructed with a range finder across the terrace situated on the northern limb of the Lumbier Anticline and supposedly

affected by northward tilting and 8 m of uplift (Insua and García-Mayordomo, 2009). This profile revealed: (1) an upper section associated with the valley margin with a northward slope of 8° ascribable to colluvium deposited after the development of the terrace; and (2) a lower section with an average slope to the north of 0.7° , with the edge of the terrace surface next to the riser situated at +40 m above the river channel, not +44 m. Subsequently, a 38 m long and 4 m deep backhoe trench was excavated with a N-S orientation and with the northern edge situated at the terrace riser (Trench TIN in Fig. 5). The trench exposed: (1) marl bedrock with a gentle N-dip (unit 1); (2) a 3.1 m thick fluvial package (units 2, 3, 4) lying on a gently south-dipping strath surface; (3) around 1 m of fine-grained slope-wash deposits with angular limestone clasts (units 5, 6); and (4) an anthropogenic fill ca. 1 m thick (unit 7). Detailed descriptions of the units are included in Fig. 5. The trench provided the following relevant factual data for assessing the previous neotectonic interpretation: (1) the terrace deposit does not show any evidence of northward tilting or deformation; (2) measurements taken with a total station (Leica TCRA1102plus) indicated that the base and the top of the terrace deposit (units 2 to 4) are situated at 31.3 m and 34.4 m above the river channel. Consequently, the terrace has neither been tectonically uplifted up to a relative height of 44 m, nor tilted to the north.

Insua and García-Mayordomo (2009), using a DEM (5 m spatial resolution), constructed a longitudinal topographic profile along an alluvial surface situated south of the Lumbier Anticline and ascribed to their T1 terrace level (+40 m). They inferred an anomalous downstream inclination of 2° for this geomorphic surface. Initially, we measured in the field a topographic profile with a range finder, which indicated the following features: (1) The alluvial surface has an average inclination of 1.2° . (2) The

alluvial surface does not have a continuous graded topography. Instead, the terrace shows four NNE-trending downstream-facing scarps 1.5 to 2.5 m high that separate eastward-stepping benches (Fig. 6). These data suggested that the investigated surface does not correspond to a single deformed terrace, but to a series of minor terraces. In order to test this hypothesis, two trenches were excavated across the two westernmost scarps (trenches TIS1 and TIS2 in Fig. 5).

Trench TIS1, 58 m long and 3 m deep, exposed the deposits of two different terraces (units 2 and 3) situated on both sides of the scarp and inset into marl bedrock. These gravelly deposits did not show any evidence of deformation (Fig. 5). Trench TIS2, 32 m long and 3.5 m deep revealed: (1) a gravelly terrace deposit (units 2,3) underlying the upper bench with a channel-like base showing a N170E orientation, measured using piercing points at both sides of the trench; and (2) below the lower part of the scarp and the inset bench, the top of the bedrock and the eastern edge of the terrace deposit corresponds to an artificial excavation surface overlain by different man-made fills (unit 4). See detailed description of units in Fig. 5. Pamplona Marls were exposed in the trench beneath the entire scarp landform, and no faults were present. The most reasonable interpretation is that there used to be two different inset terraces on both sides of the scarp and that the lower one was removed by the excavation of a gravel pit, and subsequently filled for agricultural purposes (see current analog situation in the floodplain of the Irati River in Fig. 6). The gathered geomorphic and stratigraphic evidence indicates that the previously interpreted tilted terrace, in fact corresponds to a non-deformed composite slip-off terrace comprising multiple stepped minor terraces (e.g., Fairbridge and Harris, 1968; Brackenridge, 1985). These terraces record episodic entrenchment and downstream migration of the Irati River in the inner side of a

meander with a transverse channel section, which can be observed in the current path of river (Figs. 5, 6). These geometrical relationships are equivalent to scenario J in figure 1.

The 29 km long Loiti Thrust, also known as Monreal and Lumbier fault (Puigdefábregas et al., 1976; Hernández and Simó, 1987; López et al., 1997) is a N-dipping fault with reverse displacement. It has a N120E strike that veers to a E-W orientation on its eastern sector (Figs. 3, 4). Close to the surface, the fault seems to have a steep dip as supports its linear cartographic trace (García et al., 1994; López and Solé, 1997a). In the investigated area, the Loiti Thrust places Eocene marine sediments, mainly Pamplona Marls, over Oligocene detrital formations of the Campodarbe Group (Hernández and Simó, 1987; López et al., 1997) (Fig. 3). The Lumbier Anticline, interpreted as an active fold by Insua and García-Mayordomo (2009), is the hanging-wall fault-propagation anticline of the Loiti Fault, with a steep forelimb and a more gentle backlimb (López et al., 1997). The Loiti Thrust is not included in the Quaternary Faults Database of Iberia (IGME, 2015), but it was represented in the 1:1,000,000 scale Neotectonic and Seismotectonic Map of Spain as a probable neotectonic structure, although no justification for this interpretation was provided in the accompanying report (Baena-Pérez et al., 1998).

The geomorphological map produced for this work revealed that west of Liédena village, the Loiti Thrust is overlapped by the oldest terrace (TV; +47 m) of the Irati River (Figs. 4, 5). An excavation was carried out with pick and shovel (30T 640375 / 4720251; WGS84) to obtain information on the geometrical relationships between the Loiti Thrust and the overlying terrace deposit (Fig. 7). The artificial exposure showed that the fault is truncated by an undeformed terrace deposit that carries a red, clayey, well-

developed soil profile. The basal unconformity displayed a non-displaced subhorizontal trace across the fault and the overlying gravels do not show any evidence of disturbance (i.e., reoriented fabrics, shear zones). Considering that the adjacent inset and younger terrace (TIII, +35 m; mapped as slip-off terrace in Fig. 4) was dated at ca. 117 ka by Insua and García-Mayordomo (2009), we can infer that the Loiti Thrust has not experienced any surface rupture over at least the last 117 ka. This situation fits with scenario H of figure 1.

5. The La Trinidad Thrust

The WNW-ESE-trending and S-verging La Trinidad Thrust is located in the overlapping zone between the Leyre and the Loiti thrusts (Figs. 3, 4). This is a secondary structure with a limited mappable length of at least 5 km, whose western sector is concealed by Quaternary alluvium. The thrust places the La Magdalena Anticline in the hanging-wall over the Lumbier Anticline in the footwall (López et al., 1997). The western sector of the La Trinidad Thrust is overlapped by the TIV terrace of the Irati-Salazar fluvial system, situated at around 40 m above the current channel (Figs. 4, 5). East of the terrace, on the valley margin, the thrust superposes the Guara Limestone and an unnamed unit of calcarenites, marls and marly limestones (hanging wall, Lutetian) over younger sediments of the so-called Irurozqui Flysch (footwall, Bartonian). To the west, in the scarp overlooking the floodplain, the thrust shows a smaller stratigraphic throw, juxtaposing different sections of the Irurozqui Flysch (López et al., 1997).

The surface of the terrace developed across the trace of the La Trinidad Thrust does not show any geomorphic feature indicative of recent tectonic deformation (i.e., fault scarp). However, in order to elucidate whether the complete package of Quaternary

deposits overlying the fault is not displaced (i.e., discard scenario F of figure 1), a trench was excavated intersecting perpendicularly the projection of the cartographic trace of the fault, which crops out 160 m to the east in the valley margin, and 150 m to the west in the terrace scarp (Fig. 5). The trench, 51 m long and 2.7 m deep, exposed a non-deformed terrace deposit up to 2.7 m thick unconformably overlying the faulted bedrock (Fig. 8).

Two lithostratigraphic units were differentiated in the exposed bedrock bounded by the La Trinidad Thrust, which was expressed as a damaged zone 3 m wide and truncated by the non-deformed Quaternary cover (Fig. 8). On the NE side of the fault (hanging wall) the bedrock consists of a dark grey, massive and difficult-to-excavate marly limestone, mainly with wackestone texture. This unit with subhorizontal attitude (N133E45O) and abundant millimetre-sized particles of glauconite and oxidized pyrite crystals is ascribable to the unnamed unit of calcarenites, marls and marly limestones of López et al. (1997). Around the vertical reference lines 23 and 36 the bedrock showed solutionally-enlarged fractures 20-40 cm wide filled with a reddish grey argillaceous material with carbonate nodules and subvertical veins of macrocrystalline calcite. These karstified discontinuities filled by residual material were clearly truncated by the planar strath surface (angular unconformity) lying at the base of the terrace deposit. On the SE side of the failure zone (footwall), the bedrock consists of a poorly stratified, relatively soft, light grey calcareous marl ascribable to the Iruozqui Flysch (López et al., 1997). This considerable stratigraphic throw and the well-developed shear zone indicates that the trench was excavated at a considerable distance from the fault tip. Locally, a strike and dip of bedding of N120E62SW was measured on this wall.

The fault zone shows a fault breccia comprising a large block of resistant limestone 1 m wide (ZF2) and a soft, reddish grey-brown marl with scattered angular clasts (floatbreccia) traversed by shear planes with an apparent dip of 25NE (ZF1) (Fig. 8). The northern boundary of the fault zone in contact with the hanging wall is a NE-dipping reverse fault. The terrace deposit, mainly composed of crudely stratified bouldery gravels with imbricated fabrics, lies on an erosional planar surface (rock-cut strath surface) with a slight downstream inclination and without any offset attributable to recent deformation. In the fault zone, the base of the terrace shows a more irregular geometry due to the presence of local scours 50-60 cm deep generated by differential erosion in the softer marls situated at both sides of the limestone block. Along the entire length of the trench, the gravels do not show any evidence of deformation such as shear zones or reoriented fabrics. Insua and García-Mayordomo (2009) obtained a TL age from a sample collected in this terrace level of $108 \pm 39/-22$ ka and an age of $117 \pm 44/-24$ ka from the subsequent terrace level (TIII, +36 m). Both ages, considering the error margin at one sigma, overlap at 147-93 ka. Consequently, the available data indicates that the La Trinidad Thrust has not experienced any surface rupture at least over the last 93 ka. This case illustrates scenario H of figure 1.

6. The Leyre Thrust

The Leyre Thrust is located 20 km to the south of the Itoiz Dam and 2.5 km to the north of the Yesa Dam, which is being enlarged and will create the largest reservoir of the Pyrenees (Figs. 3, 4). The Leyre Thrust was included in an early version of the Quaternary Faults Database of Iberia (QAFI v.1) (e.g., Nemser et al., 2010), referring to the work by Insua and García-Mayordomo (2009). Lacan and Ortuño (2012) included

the Leyre Thrust in a review on active tectonics in the Pyrenees quoting the “non-conclusive” studies carried out by the previous authors. Nonetheless, the Leyre Thrust was excluded from a more recent version of the Quaternary Faults Database of Iberia (QAFI v.2; IGME, 2015). The E-W-oriented and S-verging Leyre Thrust has a mappable length of 28 km and places along most of its cartographic trace resistant Cretaceous and Paleogene carbonate formations over softer Middle Eocene marls (de Rojas and Latorre, 1972; Puigdefábregas, 1975). The hanging wall of the Leyre Thrust shows a general antiformal structure with a steeper forelimb, which has been largely removed by erosion. The exposed rocks in the footwall are mainly Middle Eocene marls of the Arro-Fiscal and Pamplona formations, which show a dominant southward dip close to the thrust. In the eastern edge, the thrust grades laterally into the E-plunging pericline of the hanging-wall anticline, which is truncated by extensive non-deformed mantled pediments (Fig. 4).

The superposition along the Leyre Thrust of rocks with contrasting resistance to erosion and different structural attitude has controlled the development of the following geomorphic domains (Fig. 5): (1) The hanging wall of the thrust forms the higher part of the Leyre Range, with a broad and gently sloping northern flank roughly concordant with the structure (dip slope), and a south-facing front defined by a rock escarpment (free-face scarp) around 400 m in local relief, whose base tends to coincide with the thrust. (2) Below the rock escarpment, an extensive E-W-oriented erosional depression has been excavated in the footwall marls, drained by the Aragón River. The piedmont on the northern margin of the Aragón River valley is characterised by relatively steep colluvium-covered slopes (debris slopes) at the foot of the escarpment, that grade into mantled pediments dissected by drainages. This stepped

sequence of pediments locally merge with different terrace levels of the Aragón River (Fig. 4). The production of a detailed geomorphological map allowed the identification of six alluvial levels that record the episodic entrenchment of the Aragón River. The oldest level is represented by pediments surfaces (P6), the two youngest ones by terraces (T2, T1), whereas the remaining ones show correlative pediments and terraces (P5-P3, T5-T3). The following approximate heights above the channel were obtained for the different terrace levels: T5: +46-49 m, T4: +38-40 m; T3: +28-33 m, T2: +20-22 m; T1: +5-8 m.

Field work conducted during the elaboration of the geomorphological map allowed the identification of outcrops of the thrust plane in the canyon of the Esca River and in several quarries north of the Yesa Dam. In one of the latter outcrops, the Leyre Thrust is covered by non-deformed stratified talus deposits (30T 0649933/4722645; WGS84) (Fig. 9). The slope deposits, around 4.6 m thick, are composed of alternating, parallel-bedded decimetre-scale layers of matrix-free angular pebble gravel and thinner beds of fines with scattered clasts (Fig. 9). These are *grèze litées* mainly generated by frost shattering under past periglacial conditions (Gutiérrez, 2013; Gutiérrez and Gutiérrez, 2016). The deposit shows a syndepositional dip concordant with the inclination of the slope, which reflects the repose angle of the material at the time of its accumulation. The beds onlap the limestone of the hanging wall abutting a steep contact and recording the progressive burial of the rock scarp by the vertical accretion of the talus deposits (replacement of free-face by debris slope). Beneath the surface, the colluvium is overprinted by a calcic horizon attributable to the morphologic stage I-II of Machette (1985). The layers of the slope deposit show clear lateral continuity without any evidence of displacement over the thrust. Two charcoal samples were collected 3.2 m

(LEY-1) and 3.5 m (LEY-2) below the surface for AMS radiocarbon dating. Sample LEY-2 had insufficient organic carbon for dating. Sample LEY-1 yielded a calibrated age of 4425-4245 cal. yr BP (age range at 2 sigma; 95% probability). This geochronological information indicates the Leyre Thrust has not experienced any surface rupture since at least 4.2 ka, considering that the base of the undeformed basal part of the slope deposits may be significantly older. This case corresponds to scenario H of figure 1 and leads to an indeterminate result in case inactive faults are defined as those that have not experienced surface displacement over the last 10 kyr.

In the Leyre Thrust, we have not found old non-deformed Quaternary deposits truncating the fault. Nonetheless, there are geomorphic markers and indicators that could provide indirect evidence of activity or support inactivity. If the Leyre Thrust was considered to be an active fault, its long-term propagation could have caused the progressive steepening of the pediment surfaces developed in the piedmont. The slope of the different pediment levels would increase with their age (the older the steeper) and they would show divergent longitudinal profiles towards the mountain front (e.g., Pearce et al., 2004) (Fig. 10). Moreover, the flexure of the strata in the footwall, including beds of different rheology, could have resulted in the development of flexural-slip faults. Such faults would be expressed in the pediment surfaces as layer-parallel upslope-facing scarps and linear troughs at their foot (Rockwell et al., 1984; Kelsey et al., 2008; Walker et al., 2013; Gutiérrez et al., 2014; McCalpin et al., 2019). In order to rule out this scenario, we have constructed longitudinal profiles of pediments of different levels situated in the central sector of the Leyre Range piedmont and selecting a 1.9 km wide proximal band parallel to the trace of the thrust (Fig. 10). The profiles show a parallel pattern and similar average slopes within the

range of 7.8-13.4%, regardless of the age of the pediment levels. Moreover, the pediment surfaces do not show irregularities attributable to surface deformation related to flexural-slip faulting.

Other features that support the lack of Quaternary activity in the Leyre Thrust include:

(1) Active thrusts tend to occur at the foot of mountain fronts and are typically expressed by asymmetric convex scarps (e.g., McCalpin et al., 2019). However, the trace of the Leyre Thrust occurs at a high elevation, well above the mountain-piedmont junction, and is not expressed by scarps or convex slope breaks (Fig. 4). (2)

The activity of the thrust would cause the growth of the hanging-wall anticline located in the eastern edge of the structure and the upwarping of the extensive mantled pediment cut-across the fold. However, this pediment does not show any evidence of deformation (Fig. 4). (3) A TIV terrace (+40-45 m) of the Irati-Salazar fluvial system, situated 70 m apart from the Leyre Thrust, does not show any evidence of deformation, although this terrace seems to be located close to the fault tip (Fig. 4).

The 205 m long Peña Blanca Cave, located on the western wall of the canyon carved by the Esca River across the Leyre Range (see location in Fig. 4), was examined to check whether it contains any speleoseismological evidence (e.g., broken speleothems or with anomalous growths, collapses, discontinuities with recent displacement, liquefaction structures; Forti, 2001, 2003; Becker et al., 2006). This cave could be a good archive for the potential seismic activity sourced from the Leyre Thrust due to the following factors (Gisbert and Pastor, 2009): (1) It is located in the hanging-wall of the Leyre Thrust at a distance of just 1.4 km from the fault (30T 662720/4724215; ETRS89). (2) The cave is perched 170 m above the river channel on a steep escarpment, where ground motion is expected to experience significant topographic

amplification. For example, Gilli et al. (1999) documented that environmental effects caused by a M_w 5.2 earthquake in southern France were restricted to caves situated in elevated positions. (3) The cave, discovered in 2007, has not been disturbed by human activity.

The Peña Blanca Cave has been developed in a section of calcarenites of the Alveoline Limestone, with a ENE-WSW strike and dipping around 15N. The cave is located on the northern backlimb of the hanging wall anticline of the Leyre Thrust. It is essentially a subhorizontal and rectilinear passage controlled by subvertical WSW-ENE-trending joints. Along most of its length, the cave has a compound cross-section, comprising (1) an ellipsoidal phreatic conduit (water-table passage) with the major axis controlled by the joint; (2) a fissure in the upper part related to the solutional enlargement of the controlling joint; and (3) a rectilinear, narrow and deeply entrenched vadose channel in the lower part. Close to the entrance, the geometry of the cave has been substantially modified by condensation corrosion processes as revealed by rock pendants and solution pockets. Although speleothems are not abundant, they show significant diversity (stalactites, soda straws, eccentric stalactites, stalagmites, columns, flowstones, draperies, microgours, popcorn-type coralloids (Palmer, 2007; Gutiérrez and Gutiérrez, 2016). The cave does not show features attributable to past seismic activity. Of especial interest is the presence of unbroken soda straws, which are considered very adequate indicators of seismic activity in caves due to their fragility and high length to diameter ratio (Lacave et al., 2004; Becker et al., 2005; Kagan et al., 2005).

7. The Ruesta Fault

The Ruesta Fault is a NNE-SSW-striking and down-to-the west normal fault that crops out on the southern margin of the Aragón River valley (Fig. 3). An early geological map by De Rojas and Latorre (1972) proposed that this fault extends across the Leyre Range, offsetting the Leyre Thrust and reaching 16 km in length. Puigdefábregas (1975) and Montes (2009), in more recent and realistic geological maps restrict the Ruesta Fault (7.5 km) to the southern margin of the Aragón River valley. This is supported by the apparent lateral continuity and similar attitude of correlative distinctive beds that crop out on both sides of the Esca River valley (i.e., calcareous breccias between the Arro-Fiscal and Pamplona marls) (Fig. 11A). The Ruesta Fault, between 5.5 and 9.5 km in length, cross-cuts older contractional structures and juxtaposes along most of its cartographic trace Pamplona Marls (upthrown eastern block) against more resistant detrital sediments of the Liédena Sandstone and the Campodarbe Group (downthrown western block) (Fig. 3). According to INYPSA (2018), the master Ruesta Fault has a throw of around 650 m and is accompanied by other shorter secondary synthetic and antithetic faults with vertical separations lower than 100 m (Fig. 11A). In the downthrown block, the Liédena Sandstone is affected by a sharp drag fold reaching dips as high as 70° that rapidly attenuate away from the fault. Kinematic indicators measured on planes of secondary faults indicate dip slip displacement (rake ~90°).

The Ruesta Fault displays a very conspicuous geomorphic expression related to differential erosion (fault-line scarp) (Fig. 11A). The downthrown block, underlain by the steeply dipping (drag-folded) and resistant Liédena Sandstone forms a prominent ridge parallel to the fault, whereas higher erosion in the softer marls of the upthrown block has created an erosional depression with pediments and terraces of the Aragón River. This is an example of relief inversion that supports fault inactivity, in which the

topographically higher area is associated with the downthrown block due to the presence of more resistant rocks.

Geomorphic mapping and field surveys revealed that the Ruesta Fault is concealed by terrace T4 of the Aragón River, situated around 40 m above the submerged river channel (Fig. 11A). It crops out in a very unstable and steep scarp at the southern margin of the Yesa Reservoir. Here, the fault, steeply dipping to the W, juxtaposes different sections of the Pamplona Marls and is apparently truncated by non-deformed gravels of the T4 terrace (Fig. 11B). In order to unequivocally demonstrate that the Ruesta Fault does not displace the deposits of the T4 terrace of the Aragón River, a trench was excavated across the projected trace of the fault (Fig. 12). Owing to permit constrains, the trench was sited in a crop field close to the high-relief valley margin, where the terrace deposit is overlain by thick colluvial deposits (ca. 8 m). This setting required the excavation of a costly benched trench 56 m long, 10 m deep and 20 m wide in the upper part. The application of geophysical methods to better constrain the concealed fault was ruled out due to time limitations, the presence of thick and highly conductive argillaceous colluvium, and the same lithology at both sides of the fault (Pamplona Marls).

The exposed bedrock consisted of massive bluish grey marls with interbedded sandstone layers, in which it was possible to obtain strike and dip (or apparent dip) data (Fig. 12A). Faults were mainly identified by lateral truncation of the sandstone beds. The Ruesta Fault was expressed as a 15 m wide fault zone (fault planes, shear zones, fault breccias) in which the bedding has been largely obliterated. Between the reference lines 34 and 47 there were numerous W-dipping faults and fractures with an orientation similar to the cartographic trend of the fault. In some fault planes it was

possible to measure slickensides (striations, steps) indicative of dip-slip, down-to-the-west displacement. The master fault seems to be the one mapped at the reference line 47, as suggest a significant lithological change, with thick sandstone beds on the SE side, and a conspicuous drag fold in the downthrown block. Along the 56 m in which the trench reached the bedrock, the base of the gravelly terrace deposit showed a planar geometry (strath surface) without any evidence of deformation. Similarly, no deformations were observed in the terrace deposit (1.5-2.5 m thick), and the overlying colluvium (6-8.5 m thick). The trench clearly captured the Ruesta Fault and allowed us to confirm that the deposit of terrace T4 is not offset. With the available geochronological information (Lewis et al., 2009; Insua and García-Mayordomo, 2009; García-Ruiz et al., 2013), we can indicate that the fault has not experienced any surface rupture during at least the last 100 ka. Although faults may not rupture along their entire length during individual earthquakes (e.g. Wesnousky, 2008; DuRoss et al., 2016), for the fault to be active, the terrace should be affected by at least one faulting event considering the time elapsed since its deposition.

8. Discussion

A comprehensive seismic hazard analysis (SHA) for sensitive structures such as nuclear facilities or large dams should include fault sources, especially those located in the vicinity of the site. These may have a significant contribution to the seismic design parameters with relevant engineering and societal implications, as illustrates the results of the PSHA carried out for the Itoiz Dam, Spanish Pyrenees, which incorporated the Leyre Thrust as an active fault with a recurrence of ca. 6000 years (García-Mayordomo and Insua-Arévalo, 2011).

Before conducting a SHA for a critical structure, it is advisable to identify and characterize relevant fault sources, which may be already included in active fault databases or may be recognized through new data collection studies. Additionally, it is also highly advisable to evaluate if the postulated active faults are related to non-tectonic processes, and if the criteria used to classify them as active are valid. There are numerous scientific publications that illustrate examples of fault source characterization (e.g., McCalpin, 2009 and references therein). However, the concept of non-tectonic deformation is rarely considered, and the literature dealing with the distinction between tectonic and non-tectonic faults is very scarce (e.g., Hanson et al., 1999; Gutiérrez et al., 2012; Carbonel et al., 2013). As explained in the introduction section, numerous Quaternary deformations in the Pyrenees initially interpreted as tectonic have been subsequently ascribed to non-tectonic processes (i.e., evaporite dissolution, salt flow, sackung, landsliding). Moreover, to our knowledge, accessible works presenting studies aimed at elucidating whether a fault can be considered as active are scarce. This work illustrates a procedure, mainly based on geomorphological mapping and trenching investigations, aimed at determining whether specific faults have experienced displacement in Late Quaternary times. The approaches are similar to those applied to the characterization of confirmed active faults, although with some variations related to the aims of the investigation. The priority for fault characterization studies may be to obtain information on the most recent activity of the fault (e.g., most recent event), whereas fault activity vs. inactivity evaluation studies may require covering longer time spans to unambiguously determine if the fault has experienced any surface rupture after the chronological bound established by regulatory definition.

For the evaluation of fault activity it is essential to investigate and date Quaternary deposits, landforms and/or soils associated with the fault and with an adequate age to resolve the chronological regulatory criterion (Fig. 1). These critical sites can be identified by means of geomorphological and Quaternary geological mapping along the fault zones (strip maps) and the establishment of morpho-stratigraphic sequences (e.g., McCalpin, 2009c; Burbank and Anderson, 2012), as illustrated in figures 4 and 11. The approximate age of the target units can be estimated using multiple information, including regressions that relate age with relative heights or soil development (e.g., Moreno et al., 2012; Silva et al., 2017), long-term incision rates, and available or new geochronological data. The production of strip maps and field surveys allowed the identification of old terraces (+40-50 m) overlapping the Loiti, La Trinidad, and Ruesta faults, as well as slope deposits accumulated on the Leyre Thrust. Previous works carried out in the region ascribe an age older than 100 ka for terraces of major drainages with relative heights of around 40-50 m (e.g., Insua and García-Mayordomo, 2009; Lewis et al., 2009).

Geomorphic mapping and field surveys were not conclusive and trenching or the improvement of exposures were necessary to determine fault inactivity. Tectonic scarps may have been obliterated, and deformed Quaternary deposits may be covered by younger non-deformed units. Trenches and artificial excavations allow :(1) Exposing the fault in bedrock and unambiguously resolving the geometrical relationships with the Quaternary cover (e.g., Trenches at La Trinidad and Ruesta faults); (2) accurately measuring the relative height of the base (strath surface) and top of terrace deposits, which may be very different to that of the topographic surface due to post-terrace natural and artificial aggradation or erosion (Trench TIN); (3) determining whether the

terrace deposit has been affected by tilting (Trench TIN); (4) elucidate the nature of scarps (Trenches TIS1, TIS2); and (5) sample key stratigraphic units for dating (Fig. 9). The excavation of deep trenches may be essential to expose the deepest and oldest Quaternary deposits overlying the fault (Fig. 1F, Ruesta trench) and to determine the origin of tectonic-like features such as scarps or steep contacts (Fig. 1I, J; Trenches TIS1 and TIS2). In this regard, trenches dug across the mapped projection of a Quaternary fault which do not reach bedrock cannot be used to prove or disprove Quaternary fault activity, because there is no evidence that the trench was actually sited over the bedrock fault trace. Obviously, if the true bedrock fault lies meters to tens of meters beyond the ends of the trench, then absence of deformation in the Quaternary deposits in the trench walls is meaningless as applied to fault activity. Therefore, the available data collected by geomorphological mapping, trenching, geochronological analyses and other approaches may be insufficient to conclusively determine whether a fault is tectonic or non-tectonic, and/or if the fault is active or inactive according to regulatory definition. This epistemic uncertainty can be addressed in PSHA with different alternatives in the logic tree and assigning weights or probabilities to each of them.

Two groups of structures were analysed in this work: (1) longitudinal contractional structures related to the development of the Gavarnie Thrust, which can be considered elements of the same system (Loiti, La Trinidad, Leyre thrusts and Lumbier Anticline); and (2) a transverse normal fault that cross-cuts the earlier compressional structures (Ruesta Fault). The inactivity of the Loiti Trust, which was included in the Neotectonic and Seismotectonic Map of Spain as a probable neotectonic fault (Baena-Pérez et al., 1998), was demonstrated by non-deformed terrace deposits older than 100 ka

deposited across the fault and exposed in an improved natural outcrop. The same criterion was used to rule out activity on the 5 km long La Trinidad Thrust via trenching, although this should be considered as a secondary structure due to its limited length. Evidence used to postulate Quaternary activity on the Lumbier Anticline (Insua and García-Mayordomo, 2009), which is the hanging-wall anticline of the Loiti Thrust, was proved to be erroneous by geomorphic mapping and trenching. The terrace on the northern limb of the anticline is neither uplifted nor tilted, and the alluvial surface to the south of the anticline is not a tilted terrace, but a composite slip-off terrace comprising several minor terraces and intervening scarps. Direct evidence obtained for the Leyre Thrust has a more limited chronological range; non-faulted slope deposits indicate inactivity since at least 4.2 ka. This fault was classified as active by Insua and García-Mayordomo (2009) and incorporated in a PSHA for the Itoiz Dam with a significant contribution to the hazard results (García-Mayordomo and Insua-Arévalo, 2011). However, multiple lines of evidence support the lack of recent activity on this fault: (1) Regional cartographic relationships indicate that the activity of this structure, linked to the Gavarnie Thrust, ceased in the Early Oligocene (Teixell, 1996). (2) The other contractional structures of the system (Loiti, La Trinidad thrusts, Lumbier Anticline) should conclusive evidence of being inactive. (3) Recent GPS data indicate that this sector of the Pyrenees is currently affected by extension roughly perpendicular to the structural grain (Rigo et al., 2015; Nguyen et al., 2016). (4) Focal mechanisms in the region indicate normal and strike-slip style of faulting (Ruiz et al., 2006b; Martín et al., 2015; Rigo et al., 2015). (5) The instrumentally recorded Mw 5.4 1923 Martes earthquake occurred within the study area was related to normal faulting at depths below the basal thrust of the Pyrenees (Stitch et al., 2018). (6) The environs

of the Leyre Thrust lack the expected features of a “seismic landscape” (Michetti et al., 2005) associated with an active thrust, including the fault trace at the mountain-piedmont junction, tilted and faulted pediment surfaces in the piedmont, upwarped pediments cut-across the hanging-wall anticline, speleoseismological evidence in a high-elevation cave situated at 1.4 km distance from the fault. A deep trench excavated across the Ruesta Fault, less than 10 km long, provided conclusive evidence of inactivity since at least 100 ka.

9. Conclusions

This work illustrates, through the analysis of several faults located in the vicinity of large dams in the Pyrenees, the practicality of combining geomorphological mapping (strip maps), trenching and geochronological data for evaluating fault activity versus inactivity. Geomorphological maps allow the identification of Quaternary deposits spatially associated with the faults and establishing their relative chronology and approximate age, on the basis of chronosequences and the available geochronological data. The excavation of trenches in deposits of adequate age overlying the faults may provide conclusive evidence to determine fault activity or inactivity according to the regulatory definition (i.e., fault displacement after a specific age). Non-deformed deposits older than the chronological bound and deformed deposits younger than the age bound provide conclusive evidence of activity and inactivity, respectively. The excavation of trenches or the improvement of exposures may be indispensable for unambiguously observing the geometrical relationships between the fault and the Quaternary units, the presence or absence of deformation in the cover deposits or soils, their relative height or the origin of scarps.

The presented data reveals that previous neotectonic interpretations indicating that the Lumbier Anticline and the 28 km long Leyre Thrust are active structures were based on an incorrect interpretation of geomorphic data. Geomorphic mapping and trenches reveals that a putative tilted and uplifted terrace is not deformed and lies at the expected relative height, and that a supposedly tilted terrace is in fact a non-deformed composite slip-off terrace comprising multiple terrace treads and intervening risers. These findings have relevant implications from the seismic hazard and engineering perspective, since PSHA that incorporated the Leyre Thrust as a relevant fault source challenged the seismic design parameter of a nearby large dam.

Trenches or the improvement of exposures at sites selected on the basis of geomorphic mapping revealed that the Loiti, La Trinidad, and Ruesta faults have not experienced surface ruptures since at least 100 ka (truncated by non-deformed old terraces). The lack of activity of the Leyre Thrust is supported by non-faulted slope deposits older than 4.2 ka, lack of deformation in nearby old geomorphic surfaces, absence of speleoseismological evidence in a proximal cave, regional extension revealed by geodetic data, and earthquake focal mechanisms indicating normal and strike-slip faulting. This work illustrates the importance for seismic hazard analyses of not only characterizing active faults, but also evaluating the criteria used to postulate active seismogenic faults.

Acknowledgements

The authors are grateful to the Ebro Basin Water Authority and GEOALCALI for giving permission for publishing the work. We also thank to Fran Sanz and Fernando Palero for their assistance in the field and to the speleologist Mario Gisbert for helping in the

examination of the Peña Blanca Cave (Aragón Speleological Center). The work carried out by FG has been supported by project CGL2017-85045-P (Spanish Government). The manuscript has been improved thanks to the insightful comments provided by Edward Keller, Sarah Boulton, an anonymous reviewer, and the editor Martin Stokes.

References

- Aki, K., 1966. Generation and propagation of G waves from the Niigata earthquake of June 16, 1964. II., Estimation of earthquake movement, release energy, and stress-strain drop from G waves spectrum. *Bulletin of the Earthquake Research Institute* 44, 23-88.
- Alasset, P.J., Meghraoui, M., 2005. Active faulting in the western Pyrenees (France): Paleoseismic evidence for late Holocene ruptures. *Tectonophysics* 409, 39-54.
- Barnolas, A., Payros, A., Samsó, J.M., Serra-Kiel, J., Tosquella, J., 2004. La Cuenca surpirenaica desde el Ilerdiense medio al Priaboniense. In: Vera, J.A. (Ed.). *Geología de España*. SGE-IGME. Madrid, 313-320.
- Barnolas, A., Pujalte, V., 2004. La Cordillera Pirenaica. Definición, límites y división. In: Vera, J.A. (Ed.). *Geología de España*. SGE-IGME. Madrid, 233-241.
- Becker, A., Davenport, C.A., Eichenberger, U., Gilli, E., Jeannin, P.Y., Lacave, C., 2006. Speleoseismology: A critical perspective. *Journal of Seismology* 10, 371-388.
- Baena-Pérez, J., Moreno, F., Nozal, F., Alfaro, J.A., Barranco, L., 1992. Mapa Neotectónico y Sismotectónico de España (1:1,000,000 scale). IGME-ENRESA, Madrid.

- Bommer, J.J., Coppersmith, K.J., Coppersmith, K., Hanson, K.L., Mangongolo, A., Neveling, J., Rathje, E., Rodriguez-Marek, A., Scherbaum, F., Shelembe, R., Stafford, P.J., Strasser, F.O., 2015. A SSHAC Level 3 Probabilistic Seismic Hazard Analysis for a New-Build Nuclear Site in South Africa. *Earthquake Spectra*, 31, 661-698.
- Brakenridge, G.R., 1985. Rate estimates for lateral bedrock erosion based on radiocarbon ages, Duck River, Tennessee. *Geology* 13, 111-114.
- Brune, J.N., 1993. The seismic hazard at Tehri dam. *Tectonophysics*, 218, 281-286.
- Burbank, D.W., Anderson, R.S., 2012. *Tectonic Geomorphology*. Wiley-Blackwell, Chichester, 454 p.
- Carbonel, D., Gutiérrez, F., Linares, R., Roqué, C., Zarroca, M., McCalpin, J., Guerrero, J., Rodríguez, V., 2013. Differentiating between gravitational and tectonic faults by means of geomorphological mapping, trenching and geophysical surveys. The case of the Zenzano Fault (Iberian Chain, N Spain). *Geomorphology* 189, 93-108.
- CNEGP, 1999. *Guía Técnica de Seguridad de Presas Nº 3. Estudios geológicos-geotécnicos y de prospección de materiales*, Colegio de Ingenieros de Caminos Canales y Puertos, 189 p.
- de Rojas, B., Latorre, F., 1972. *Mapa Geológico de Sigués (175) a escala 1:50.000*. IGME. Madrid, 15 p.
- DuRoss, C.B., Personious, S.F., Crone, A.J., Olig, S.S., Hylland, M.D., Lund, W.R., Schwartz, D.P., 2016. Fault segmentation: New concepts from the Wasatch Fault Zone, Utah, USA. *Journal of Geophysical Research: Solid Earth* 121, 1131-1157.
- Fabregat, I., Gutiérrez, F., Roqué, C., Comas, X., Zarroca, M., Carbonel, D., Guerrero, J., Linares, R., 2017. Reconstructing the internal structure and long-term evolution of

- hazardous sinkholes combining trenching, electrical resistivity imaging (ERI) and ground penetrating radar (GPR). *Geomorphology* 285, 287-304.
- Fairbridge, R.W., Harris, S.A., 1968. Slip-off slope. In: Fairbridge, R.W. (Ed.). *The Encyclopedia of Geomorphology*. Dowden, Hutchinson and Ross. Stroudsburg, 996-998.
- Forti, P., 2001. Seismotectonic and paleoseismic studies from speleothems: The state of the art. *Netherlands J. Geosciences* 80, 175-185.
- Forti, P., 2003. Paleotectonics from speleothems. In: Gunn, J. (Ed.). *Encyclopedia of Caves and Karst Science*. Fitzroy Dearborn, New York, 565-566.
- Fraser, W.A., 2001. California Division of safety of dams fault activity guidelines. California Department of Water Resources, Division of Safety of Dams, California.
- García, J., del Valle, J., Escuer, J., Sarasa, L., Artieda, J., Sánchez, E., Coullaut, J.L., 1994. Mapa Geológico de Monreal (142-III) a escala 1:25.000. Comunidad Foral de Navarra. Pamplona, 36 p.
- García-Mayordomo, J., Insua-Arévalo, J.M., 2011. Seismic hazard assessment for the Itoiz dam site (Western Pyrenees, Spain). *Soil Dynamics and Earthquake Engineering* 31, 1051-1063.
- García-Ruiz, J.M., Martí-Bono, C., Peña-Monné, J.L., Sancho, C., Rhodes, E.J., Valero-Garcés, B., González-Sampériz, P., Moreno, A., 2013. Glacial and fluvial deposits in the Aragón valley, central-western Pyrenees: Chronology of the Pyrenean Late Pleistocene glaciers. *Geografiska Annaler: Series A, Physical Geography* 95, 15-32.
- Gilli, E., Levret, A., Sollogoub, P., Delange, P., 1999. Research on the February 18, 1996 earthquake in the caves of Saint-Paul-de-Fenouillet area, (eastern Pyrenees, France). *Geodinamica Acta* 12, 143–158.

- Gisbert, M., Pastor, M., 2009. Cuevas y Simas de la Provincia de Zaragoza. Centro de Espeleología de Aragón, Zaragoza, 479 p.
- González de Vallejo, L.; Rodríguez, J.A.; Seisdedos, J.; Insua, J.M.; García-Mayordomo, J.; Blázquez, R.; López, S., 2010. Análisis y seguimiento del Embalse de Itoiz: Estabilidad de laderas, sismicidad y condiciones geotécnicas. Technical Report 2007-2009.
- Goula, X., Olivera, C., Fleta, J., Grellet, B., Lindo, R., Rivera, L.A., Cisternas, A., Carbon, D., 1999. Present and recent stress regime in the eastern part of the Pyrenees. *Tectonophysics* 308, 487-502.
- Gutiérrez, F., Carbonel, D., Kirkham, R.M., Guerrero, J., Lucha, P., Matthews, V., 2014. Can flexural-slip faults related to evaporite dissolution generate hazardous earthquakes? The case of the Grand Hogback Monocline of west-central Colorado. *GSA Bulletin* 126, 1481-1494.
- Gutiérrez, F., Fabregat, I., Roqué, C., Carbonel, D., Guerrero, J., García-Hermoso, F., Zarroca, M., Linares, R., 2016. Sinkholes and caves related to evaporite dissolution in a stratigraphically and structurally complex setting, Fluvia Valley, eastern Spanish Pyrenees. Geological, geomorphological and environmental implications. *Geomorphology* 267, 76-97.
- Gutiérrez, F., Gutiérrez, M., 2016. *Landforms of the Earth. An Illustrated Guide.* Springer, Dordrecht, 270 p.
- Gutiérrez, F., Linares, R., Roqué, C., Zarroca, M., Carbonel, D., Rosell, J., Gutiérrez, M., 2015. Large landslides associated with a diapiric fold in Canelles Reservoir (Spanish Pyrenees): Detailed geological-geomorphological zapping, trenching and electrical resistivity imaging. *Geomorphology* 241, 224-242.

- Gutiérrez, F., Linares, R., Roqué, C., Zarroca, M., Rosell, J., Galve, J.P., Carbonel, D. 2012. Investigating gravitational grabens related to lateral spreading and evaporite dissolution subsidence by means of detailed zapping, trenching, and electrical resistivity tomography (Spanish Pyrenees). *Lithosphere* 4, 331-353.
- Gutiérrez, F., Ortuño, M., Lucha, P., Guerrero, J., Acosta, E., Coratza, P., Piacentini, D., Soldati, M., 2008. Late Quaternary episodic displacement on a sackung scarp in the central Spanish Pyrenees. Secondary paleoseismic evidence? *Geodinámica Acta* 21, 4, 187-202.
- Gutiérrez, M., 2013. *Geomorphology*. CRC Press/Balkema, Leiden, 1017 p.
- Gutiérrez-Santolalla, F., Acosta, E., Ríos, S., Guerrero, J., Lucha, P., 2005. Geomorphology and geochronology of sackung features (uphill-facing scarps) in the Central Spanish Pyrenees. *Geomorphology* 69, 298-314.
- Hanson, K.L., Kelson, K.I., Angell, M.A., Lettis, W.R. (Eds.), 1999. Techniques for identifying faults and determining their origins. U.S. Nuclear Regulatory Commission. Washington, contract report NUREG/CR-5503, 186 p. plus appendices.
- Hernández, A., Simó, A., 1987. Mapa Geológico de Sangüesa (174) a escala 1:50.000. IGME. Madrid, 55 p.
- IAEA, 2015. The Contribution of Palaeoseismology to Seismic Hazard Assessment in Site Evaluation for Nuclear Installations. IAEA TECDOC No. 1767, 208 p.
- ICOLD, 1998. Neotectonics and Dams. Guidelines and case histories. International Commission on Large Dams, Bulletin 112, 95 p.
- ICOLD, 2016. Selecting seismic parameters for large dams, guidelines. Committee on Seismic Aspects of Dam Design. International Commission on Large Dams, Bulletin 148.

- IGME, 2015. QAFI v.3: Quaternary Active Faults Database of Iberia.
<http://info.igme.es/QAFI>
- Insua, J.M., García-Mayordomo, J., 2009. Upper Pleistocene tectonic activity in the central Pyrenees Range (Navarra, N Spain). In: Pérez-López, R., Grützner, C., Lario, J., Reicherter, K., Silva, P. (Eds.). *Archeoseismology and Paleoseismology in the Alpine-Himalayan Collisional Zone*. 1st INQUA-IGCP 567 International Workshop on Earthquake Archeology and Paleoseismology, 60-62.
- INYPSA, 2018. Cartografía geológica del Proyecto Muga y análisis de fallas singulares. Technical Report, 39 p.
- Kagan, E.J., Agnon, A., Bar-Matthews, M., Ayalon, A., 2005. Dating large infrequent earthquakes by damaged cave deposits. *Geology* 33, 261–264.
- Kelsey, H.M., Sherrod, B.L., Nelson, A.R., Brocher, T.M., 2008. Earthquakes generated from bedding plane-parallel reverse faults above an active wedge thrust, Seattle fault zone. *Geological Society of America Bulletin* 120, 1581-1597.
- Lacan, P., Ortuño, M., 2012. Active tectonics of the Pyrenees: A review. *Journal of Iberian Geology* 38, 9-30.
- Lacave, C., Koller, M.G., Egozcue, J.J., 2004. What can be concluded about seismic history from broken and unbroken speleothems? *Journal of Earthquake Engineering* 8, 431–455.
- Lewis, C.J., McDonald, E.V., Sancho, C., Peña, J.L., Rhodes, E.J., 2009. Climatic implications of correlated Upper Pleistocene glacial and fluvial deposits on the Cinca and Gállego Rivers (NE Spain) based on OSL dating and soil stratigraphy. *Global and Planetary Change* 67, 141-152.

- López, S., Solé, J., 1997a. Mapa Geológico de Tiermas (175-I) a escala 1:25.000. Comunidad Foral de Navarra. Pamplona, 155 p.
- López, S., Solé, J., 1997b. Mapa Geomorfológico de Lumbier (174-II) a escala 1:25.000. Comunidad Foral de Navarra. Pamplona, 177 p.
- López, S., Solé, J., Galán, G., 1997. Mapa Geológico de Lumbier (174-II) a escala 1:25.000. Comunidad Foral de Navarra. Pamplona, 177 p.
- López-Martínez, J., 1986. Geomorfología del Macizo kárstico de la Piedra de San Martín. Tesis Doctoral. Universidad de Zaragoza, 529 p.
- Lucha, P., Gutiérrez, F., Galve, J.P., Guerrero, J., 2012. Geomorphic and stratigraphic evidence of incision-induced halokinetic uplift and dissolution subsidence in transverse drainages crossing the evaporite-cored Barbastro-Balaguer Anticline (EbroBasin, NE Spain). *Geomorphology* 171-172, 154-172.
- Machette, M.N., 1985. Calcic soils of the southwestern United States. In: Weide, D.L. (Ed.). *Quaternary soils and Geomorphology of the American Southwest*. Geological Society of America, Special Paper 203, 1-21.
- Martín, R., Stich, D., Morales, J., Mancilla, F., 2015. Moment tensor solutions for the Iberian_Maghreb region during the IberArray deployment (2009-2013). *Tectonophysics* 663, 261–274.
- Martínez-Solares, J.M., Mezcuá, J., 2002. Catálogo sísmico de la Península Ibérica (880 a.c.-1900). Instituto Geográfico Nacional, 253 p.
- McCalpin, J.P., 2009a. Application of paleoseismic data to seismic hazard assessment and neotectonic research. In: McCalpin, J.P. (Ed.) *Paleoseismology*. Academic Press-Elsevier, 1-106.

- McCalpin, J.P., 2009b. Field techniques in paleoseismology. Terrestrial environments. In McCalpin, J.P. (Ed.) Paleoseismology. Academic Press-Elsevier, 29-118.
- McCalpin, J.P. (Ed.), 2009. Paleoseismology. Elsevier, Amsterdam, 613 p.
- McCalpin, J.P., Corominas, J. 2019, in review. Postglacial deformation history of sackungen on the northern slope of Pic d'Encampadana, Andorra. Geomorphology.
- McCalpin, J.P., Gutierrez, F., Bruhn, R.L., Guerrero, J., Pavlis, T.L., Lucha, P., 2019, in preparation. Tectonic Geomorphology and late Quaternary deformation on the Ragged Mountain Fault, Yakutat Microplate, South Coastal Alaska.
- Michetti, A.M., Audemard, F., Marco, S., 2005. Future trends in paleoseismology: Integrated study of the seismic landscape as a vital tool in seismic hazard analyses. Tectonophysics 408, 3-21.
- Montes, M.J., 2009. Estratigrafía del Eoceno-Oligoceno de la Cuenca de Jaca. Sinclinatorio del Guarga. Instituto de estudios Altoaragoneses. Colección de Estudios Altoaragoneses 59, 355 p.
- Moreno, D., Falguères, C., Pérez-González, A., Duval, M., Voinchet, P., Benito-Calvo, A., Ortega, A.I., Bahain, J.J., Sala, R., Carbonell, E., Bermúdez de Castro, J.M., Arsuaga, J.L., 2012. ESR chronology of alluvial deposits in the Arlanzón valley (Atapuerca, Spain): Contemporaneity with Atapuerca Gran Dolina site. Quaternary Geochronology 10, 418-423.
- Nemser, E.S., García-Mayordomo, J., Cabral, J., Fonseca, J.F.B.D., Martínez-Díaz, J.J., Vilanova, S., and the 2010 Working Group of Iberian Seismogenic Sources, 2010. Compilation of parametrized seismogenic sources in Iberia for the SHARE European-scale seismic source model. In: Insua-Arévalo, J., Martín-González, F. (Eds.). Primera Reunión Ibérica sobre Fallas Activas y Paleoseismología, 201-204.

- Nguyen, H.N., Vernant, P., Mazzotti, S., Khazaradze, G., Asensio, E., 2016. 3-D GPS velocity field and its implications on the present-day post-orogenic deformation of the Western Alps and Pyrenees. *Solid Earth* 7, 1349-1363.
- Olivera, C., Redondo, E., Lambert, J., Riera Melis, A., Roca, A., 2006. Els terratrèmols dels segles XIV i XV a Catalunya. Institut Cartogràfic de Catalunya, Cataluña, Monografies 30, 407 p.
- Ortuño, M., 2009. Deformación active en el Pirineo central: La falla Norte de la Maladeta y otras fallas activas. PhD. Thesis. University of Barcelona, 346 p.
- Palmer, A.N., 2007. *Cave Geology*. Allen Press, Lawrence, 454 p.
- Pearce, S.A., Pazzaglia, F.J., Eppes, M.C., 2004. Ephemeral stream response to growing folds. *Geological Society of America Bulletin* 116, 1223-1239.
- Perea, H., 2009. The catalan seismic crisis (1427 and 1428): Geological sources and earthquake triggering. *Journal of Geodynamics* 47, 259-270.
- Philip, H., Bousquet, J.C., Escuer, J., Fleta, J., Goula, X., Grellet, B., 1992. Présence de failles inverses d'âge quaternaire dans l'Est des Pyrénées: implications sismotectoniques. *Comptes Rendus de l'Académie de Sciences* 314, 1239-1245.
- Puigdefàbregas, C., 1975. La sedimentación molásica en la Cuenca de Jaca. Instituto de Estudios Pirenaicos, Jaca, 188 p.
- Puigdefàbregas, C., Rojas, B., Sánchez, I., del Valle, J., 1976. Mapa Geológico de Aoiz (142) a escala 1:50.000. IGME. Madrid, 27 p.
- Rigo, A., Vernant, P., Feigl, K.L., Goula, X., Khazaradze, G., Talaya, J., Morel, L., Nicolas, J., Baize, S., Chéry, J., Sylvander, M., 2015. Present-day deformation of the Pyrenees revealed by GPS surveying and earthquake focal mechanisms until 2011. *Geophysical Journal International* 201, 947-964.

- Rockwell, T.K., Keller, E.A., Clark, M.N., Johnson, D.L., 1984. Chronology and rates of faulting of Ventura River terraces, California: Geological Society of America Bulletin, 95, 1466-1474.
- Rosell, J., Linares, R., Llompart, C., 2001. El "Garumniense" prepirenaico. Revista de la Sociedad Geológica de España 14, 47-56.
- Rosell, L., Pueyo, J.J., 1997. Second marine evaporitic phase in the south Pyrenean foredeep: The Priabonian potash basin (Late Eocene: Autochthonous-Allochthonous Zone). In: Busson G., Schreiber, B.C. (Eds.). Sedimentary deposition in rift and foreland basins in France (Paleogene and Lower Neogene). Columbia University Press, New York, 358-387.
- Ruiz, M., Gaspà, O., Gallart, J., Díaz, J., Pulgar, J.A., García-Sansegundo, J., López-Fernández, C., González-Cortina, J.M., 2006a. Aftershocks series monitoring of the September 18, 2004 M=4.6 earthquake at the western Pyrenee: A case of reservoir-triggered seismicity? Tectonophysics 424, 223-243.
- Ruiz, M., Gallart, J., Díaz, J., Olivera, C., Pedreira, D., López, C., González-Cortina, J.M., Pulgar, J.A., 2006b. Seismic activity at the western Pyrenean edge. Tectonophysics, 412, 217-235.
- Sébier, M., Meyer, B., 2008. Comité de Pilotage de NEOPAL. Visite de terrain: rapport de mission sur le terrain dans les Pyrenees centrales du comite de pilotage da la base neopal le Jeudi 23 Octobre 2008. Technical report, 12 p.
- Silva, P.G., Roquero, E., López-Recio, M., Huerta, P., Martínez-Graña, A., 2017. Chronology of fluvial terrace sequences for large Atlantic rivers in the Iberian Peninsula (Upper Tagus and Duero drainage basins, Central Spain). Quaternary Science Reviews 166, 188-203.

- Slemmons, D.B., 1982. Determination of the design earthquake magnitudes for microzonation. Proceedings of the 3rd International Earthquake Microzonation Conference. Seattle, Vol. 1, 119-130.
- Stich, D., Martín, R., Batlló, J., Macià, R., Mancilla, F., Morales, J., 2018. Normal faulting in the 1923 Berdún earthquake and postorogenic extension in the Pyrenees. *Geophysical Research Letters* 45, 3026–3034.
- Teixell, A., 1996. The Ansó transect of the southern Pyrenees: Basement and cover thrust geometries. *Journal of the Geological Society* 153, 301-310.
- Tosun, H., Zorluer, I, Orhan, A., Seyrek, E., Savas, H., Turkoz, M., 2007. Seismic hazard and total risk analyses for large dams in Euphrates basin, Turkey. *Engineering Geology* 89 155-170.
- Walker, R.T., Khatib, M.M., Bahroudi, A., Rodés, A., Schnable, C., Fattahi, M., Talebian, M., Bergman, E., 2013. Co-seismic, geomorphic, and geologic fold growth associated with the 1978 Tabas-e-Golshan earthquake fault in eastern Iran. *Geomorphology* 237, 98-118.
- Wells, D. L., Coppersmith, K.J., 1994. New empirical relationships among magnitude, rupture length, rupture area, and surface displacement. *Bulletin of the Seismological Society of America* 84, 974-1002.
- Wesnousky, S.G., 2008. Displacement and geometrical characteristics of earthquake surface ruptures: issues and implications for seismic-hazard analysis and the process of earthquake rupture. *Bulletin of the Seismological Society of America* 98, 1609-1632.
- Wieland, M. Chen, H., 2009. Lessons learnt from the Wenchuan earthquake. *International Journal of Water Power and Dam Construction*.

<https://www.waterpowermagazine.com/features/featurelessons-learnt-from-the-wenchuan-earthquake/>

Wieland, M., 2014. Seismic hazard and seismic design and safety aspects of large dam projects. In: Ansal, A. (Ed.). Perspectives on European Earthquake Engineering and Seismology. Geotechnical, Geological and Earthquake Engineering. Springer, Cham, 627-650.

Wieland, M., Brenner, R.P., Bozovic, A., 2008. Potentially active faults in the foundations of large dams. Part II: Design aspects of dams to resist fault movements. 14th World Conference on Earthquake Engineering. Beijing, 8 p.

Youngs, R.R., Coppersmith, K.J., 1985. Implication of fault slip rates and earthquake recurrence models to probabilistic seismic hazard estimates. Bulletin of the Seismological Society of America 75, 939-964.

Zarroca, M., Linares, R., Bach, J., Roqué, C., Moreno, V., Font, L., Baixeras, C., 2012. Integrated geophysics and soil gas profiles as a tool to characterize active faults: the Amer fault example (Pyrenees, Spain). Environmental Earth Science 67, 889-910.

Figure captions

Figure 1. Different stratigraphic, geomorphic, structural and chronologic scenarios and their possibilities and limitations for unambiguously determining if a fault meets the regulatory definition for active fault based on the age of the latest displacement (35 ka in this example). Explanations given in the text. The complexity associated with soil profiles is illustrated in **figure 2**.

Figure 2. Diagram illustrating how the determination of fault activity using soil profiles depends on multiple factors, in addition to the age at which soil development began. This Gedanken experiment assumes (1) onset of soil development at 50 ka; (2) the soil rate development indicated in the legend; (3) fault throw equal to half the thickness of fully developed soil profile; (4) erosion in the footwall block (FW) to the level of the downthrown block.

Figure 3. Geological sketch of the investigated area, showing the distribution of the analysed faults and folds, and the main drainages that have generated the Quaternary alluvial levels used as geomorphic markers. Lithostratigraphic sketch modified from (Barnolas et al., 2004) of the Jaca-Pamplona Basin. Green color in the map corresponds to Cretaceous and Paleocene sediments deposited before the development of the Jaca-Pamplona Basin. The poorly constrained location of the epicenter of the 1923 Martes (or Berdún) earthquake is indicated (IGN earthquake catalogue).

Figure 4. Geomorphological map of the alluvial levels (pediments and terraces) developed by the Irati-Salazar fluvial system upstream and downstream of the Lumbier

Anticline, and the Aragón River on the northern margin of its valley. The map shows some cartographic relationships between the analysed structures and Quaternary deposits.

Figure 5. Logs of trenches TIN, TIS1, TIS2, and their location, including also trench TIT, with respect to the different geological structures.

Figure 6. Oblique view of the composite slip-off terrace developed in the inner side of a meander of the Irati River, showing a stepped sequence of minor terraces separated by transverse scarps (terrace risers). The approximate location of trenches TIS1 and TIS2 excavated across the scarps is indicated (red lines).

Figure 7. Hand-dug artificial exposure showing the Loiti Thrust truncated by undeformed deposits of the oldest terrace (TV) of the Irati River. Eocene marine marls on the upthrown block and red Oligocene detrital sediments of the Campodarbe Group in the footwall. Segments of pole are 10 cm long.

Figure 8. Log of trench TIT excavated in terrace TIV across the projected trace of La Trinidad Thrust. See location of trench in figure 4. The photographs show a general view of the La Trinidad Thrust and the trench excavated across its projected trace (left), and a the fault zone overlain by non-deformed terrace deposits, filling local scours in soft material at both sides of a resistant limestone block.

Figure 9. A) Artificial exposure of the Leyre Thrust buried by a non-deformed stratified slope deposit (*grèze letées*). B) General view of the outcrop showing the position of charcoal samples collected for radiocarbon dating.

Figure 10. A) Idealized morphostructural sketch of a hypothetical active Leyre Thrust with oversteepened pediments showing diverging longitudinal profiles towards the mountain front. Pediment surfaces are offset by flexural-slip faults in the piedmont. The amount of deformation increases with the age of the pediment levels. B) Trace of longitudinal profiles (indicated by numbers) along different pediment levels on a shaded relief model. C) Longitudinal profiles along different pediment levels showing a parallel pattern.

Figure 11. A) Morphostructural strip map of the Ruesta Fault, showing the location of the trench excavated in terrace T4 across the projected trace of the fault. B) Outcrop on the southern margin of the Yesa Reservoir, where the Ruesta Fault is apparently truncated by non-deformed gravels of the terrace T4 of the Aragón River.

Figure 12. The Ruesta Fault trench. A) Log of the southern wall showing the fault zone truncated by non-deformed terrace deposits. B) Surface model generated with drone data showing the trench and the exposure of the fault in the southern scarp margin of the Yesa Reservoir. C) View of the trench from the SE edge. D) General view of the trench showing the fault-line scarp associated with the Ruesta Fault, with a prominent ridge of Liédena Sandstone in the downthrown block (relief inversion).

Highlights

Evaluation of fault activity vs. inactivity by geomorphic mapping and trenching

Limitations of soils, Quaternary deposits and numerical ages for determining fault activity

The importance of trenching for reducing epistemic uncertainty

Geomorphology plays a key role in the identification of seismogenic fault sources

The impact of incorrect geomorphic interpretations on seismic hazard analyses

ACCEPTED MANUSCRIPT





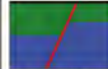





Bedrock		Soil (S)			Quaternary deposit (QD)				
Scarp					Scarp		Scarp		
Faulted bedrock			Faulted Q deposit or soil				Non-faulted Q cover		
A	B	C	D	E	F	G	H	I	J
Faulted bedrock	Faulted bedrock Scarp	Faulted bedrock Unfaulted soil	Faulted soil	Faulted QD	Faulted QD Unfaulted QD	Faulted QD Fault scarp	Faulted bedrock Unfaulted QD	Unfaulted QD Erosional scarp	Unfaulted QDs Erosional scarp
									
INDETERMINATE	INDETERMINATE erosional scarp? age of scarp?	S > 35 ka INDETERMINATE S < 35 ka INDETERMINATE	S < 35 ka ACTIVE S > 35 ka INDETERMINATE	QD < 35 ka ACTIVE QD > 35 ka INDETERMINATE	Lower QD < 35 ka ACTIVE Lower QD > 35 ka INDETERMINATE Upper QD > 35 ka INACTIVE	QD < 35 ka ACTIVE QD > 35 ka INDETERMINATE	QD > 35 ka INACTIVE	NO FAULT	NO FAULT

Figure 1

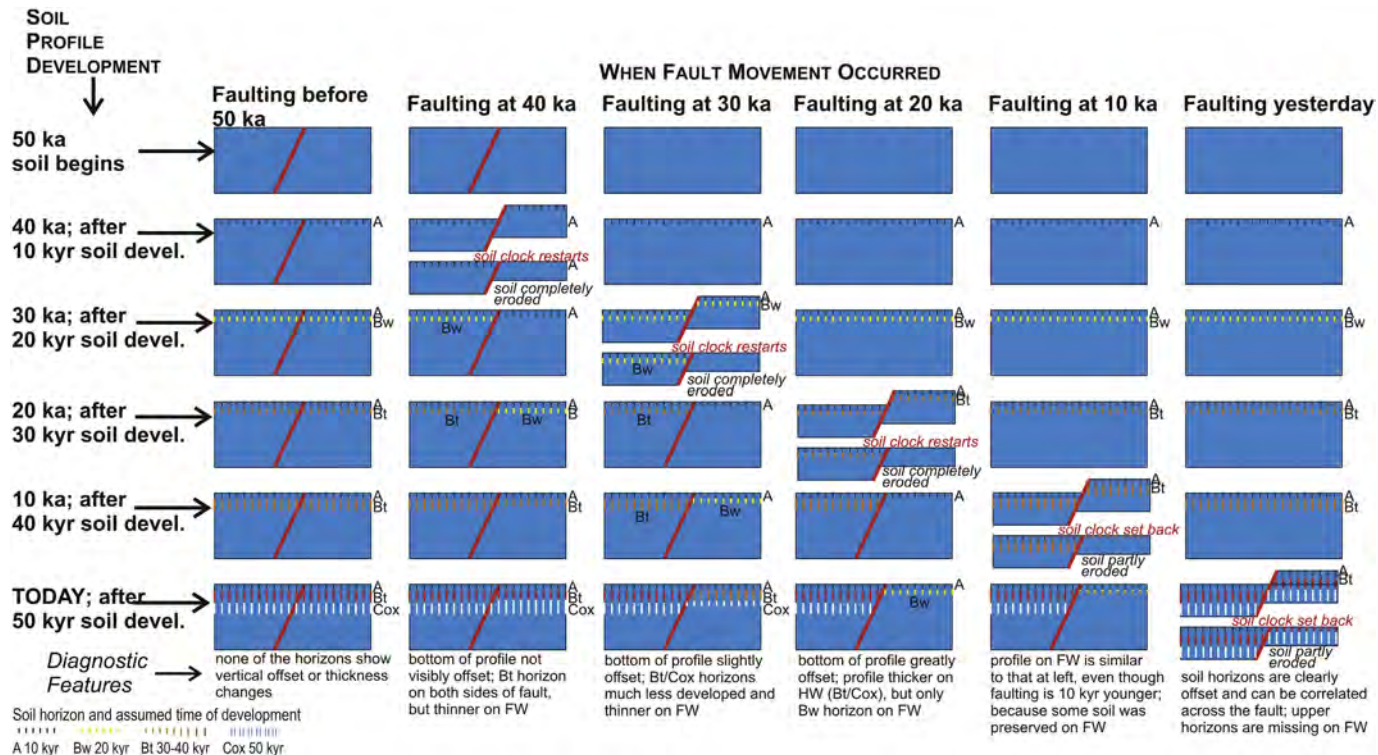


Figure 2

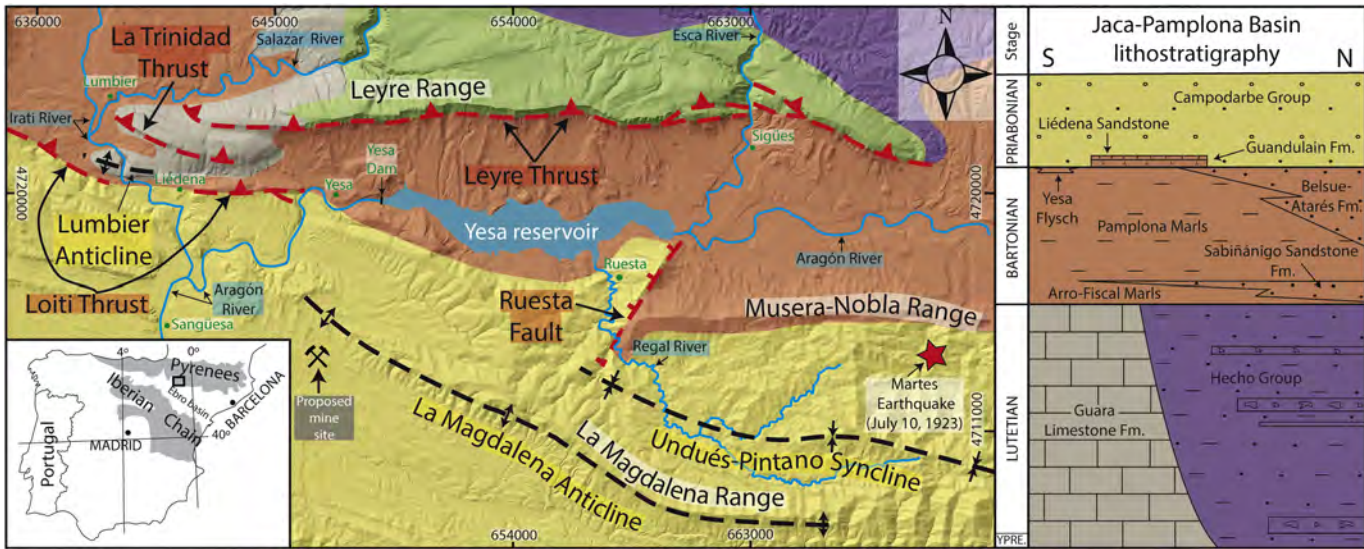


Figure 3

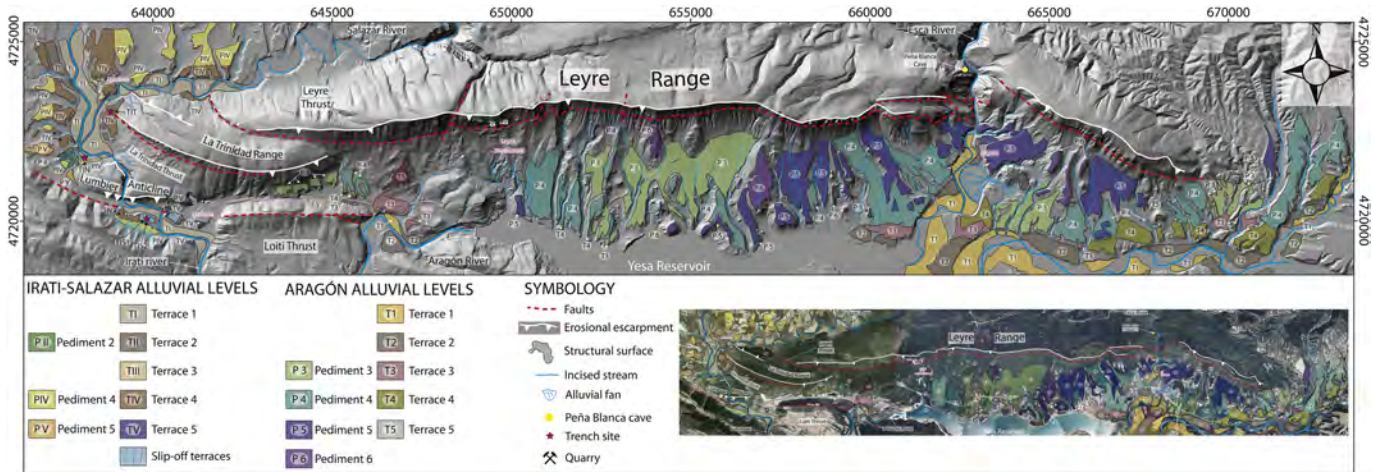
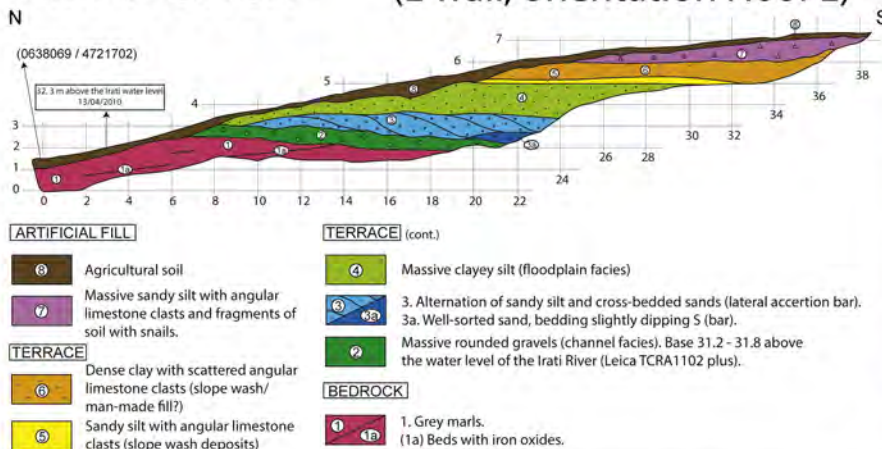


Figure 4

TIN Trench

(E wall, orientation N007E)

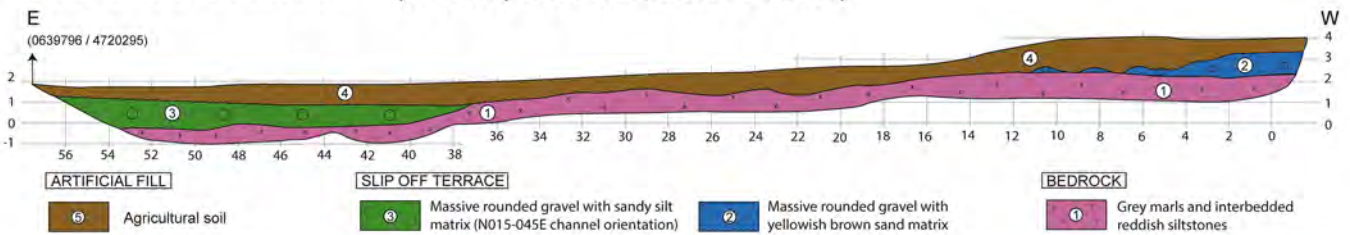


LOCATION MAP



TIS1 Trench

(S wall, orientation N120E)



TIS2 Trench

(S wall, orientation N105E)

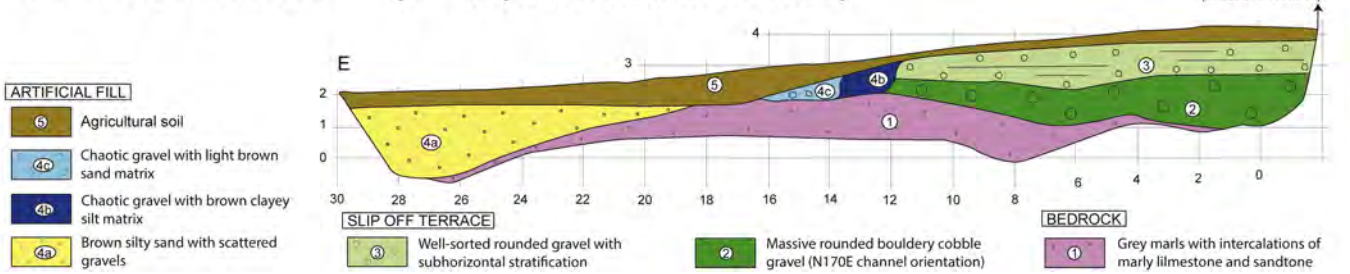


Figure 5

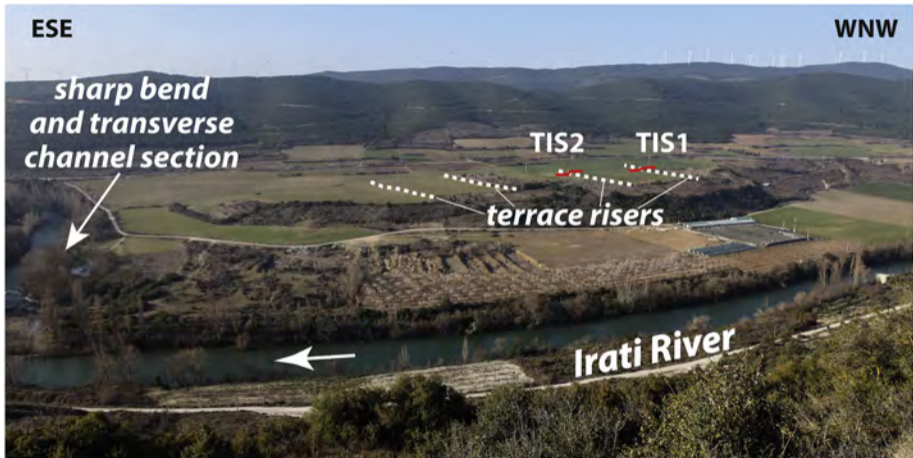
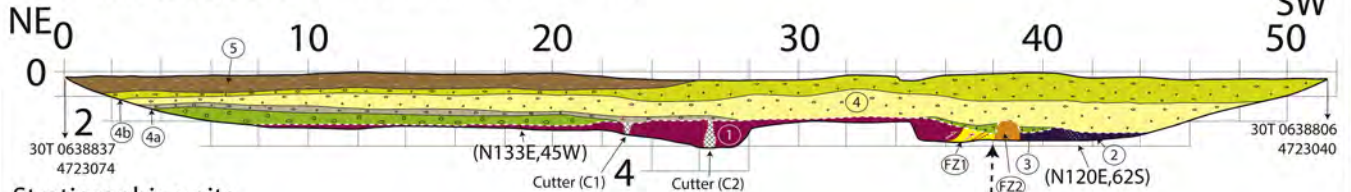


Figure 6



Figure 7

TIT Trench (SE wall, orientation N40E)



Stratigraphic units

Cover

- ⑤ Massive reddish brown clayey silt with scattered rounded clasts (sheet wash deposit)
- ④b } Crudely bedded, moderately sorted, polymictic, clast-supported, sub-rounded bouldery
 ④ } cobble-pebble gravel with matrix consisting of sand a fine gravel. (4a) Tabular bed blackish
 ④a } in colour (manganese oxides). (4b) Reddish brown argillic horizon (Bt, illuviation horizon)
 atop calcic horizon (Bk) with clasts coated by secondary calcium carbonate.
- ③ Massive, poorly sorted, polymictic, subrounded bouldery cobble-pebble gravel with chaotic fabrics (infill of local scours generated by differential erosion)

Fault zone

- FZ1 Hard block of limestone ascribed to unit 1 and bounded by fault planes.
- FZ2 Gray and reddish brown soft marl with angular boulders of calcareous marls and NE-dipping shear planes (fault floatbreccia).

Bedrock

- ② Poorly bedded, light grey calcareous marl much softer than unit 1 with fragmentary fossils coated by iron oxides. Unit 12 of López et al. (1997).
- ① Poorly bedded, hard, dark grey marly limestone (wackestone and mudstone) with millimetre-sized glauconite particles and oxidized pyrite crystals. Unit 8 of López et al. (1997).



Figure 8

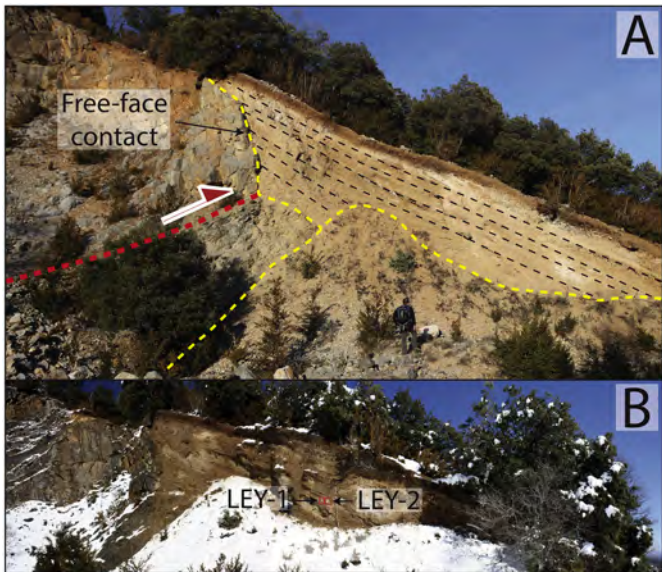


Figure 9

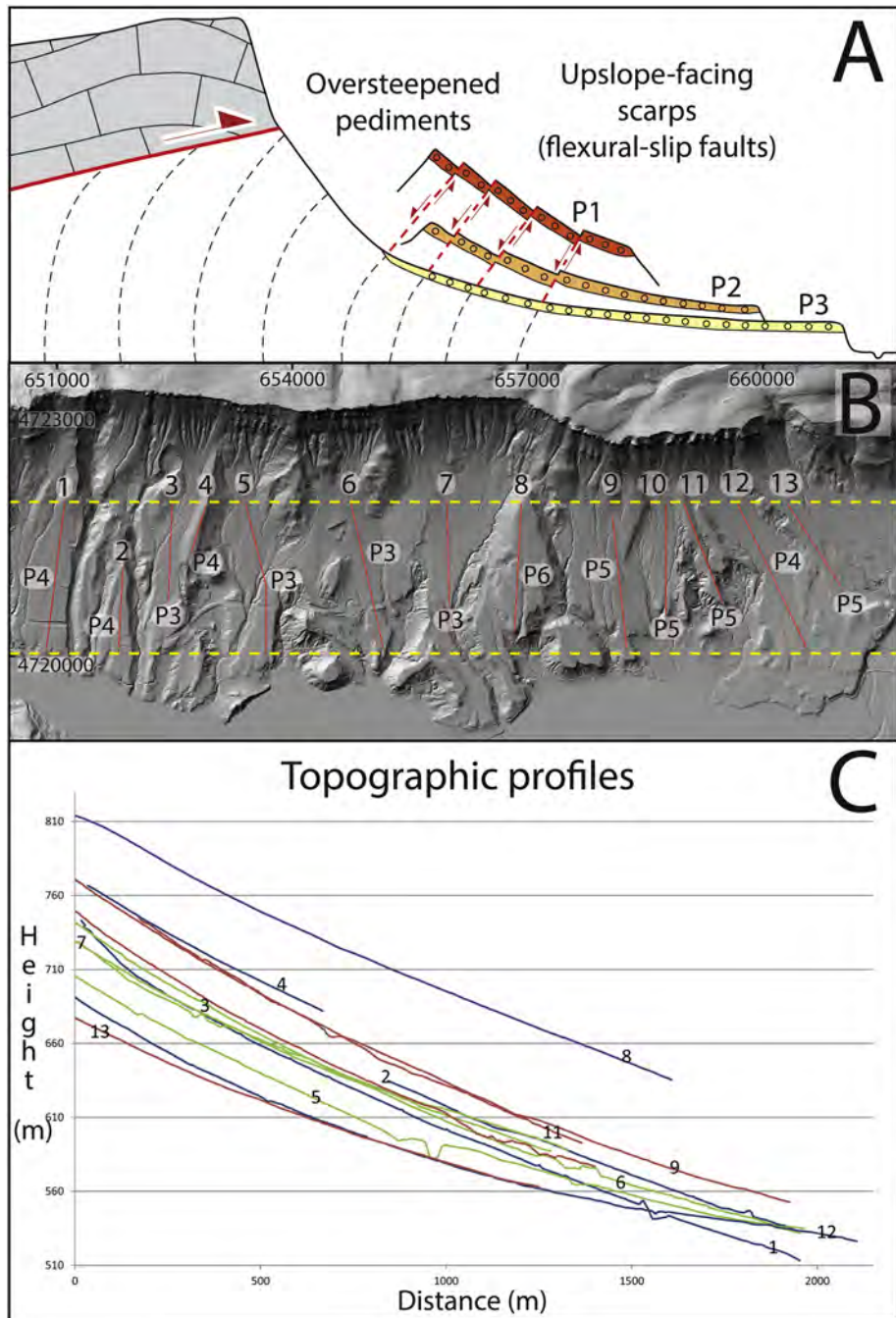


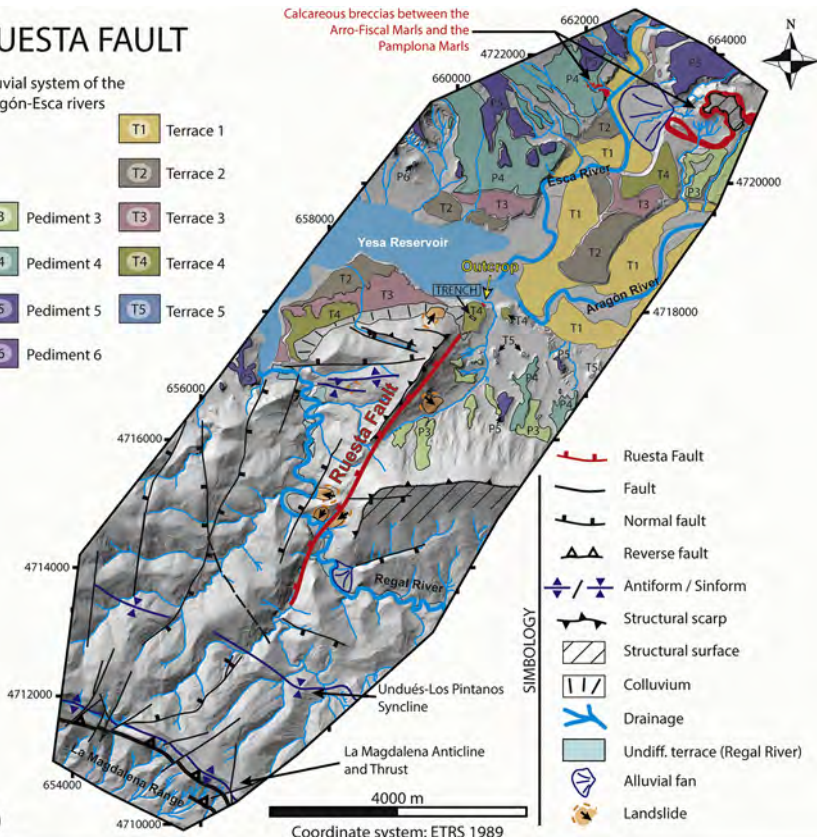
Figure 10

RUESTA FAULT

Alluvial system of the Aragón-Esca rivers

- T1 Terrace 1
- T2 Terrace 2
- T3 Terrace 3
- T4 Terrace 4
- T5 Terrace 5
- P3 Pediment 3
- P4 Pediment 4
- P5 Pediment 5
- P6 Pediment 6

Calcareous breccias between the Arro-Fiscal Marls and the Pamplona Marls



- SIMBOLY**
- Ruesta Fault
 - Fault
 - Normal fault
 - Reverse fault
 - Antiform / Sinform
 - Structural scarp
 - Structural surface
 - Colluvium
 - Drainage
 - Undiff. terrace (Regal River)
 - Alluvial fan
 - Landslide

(A)

Outcrop



(B)

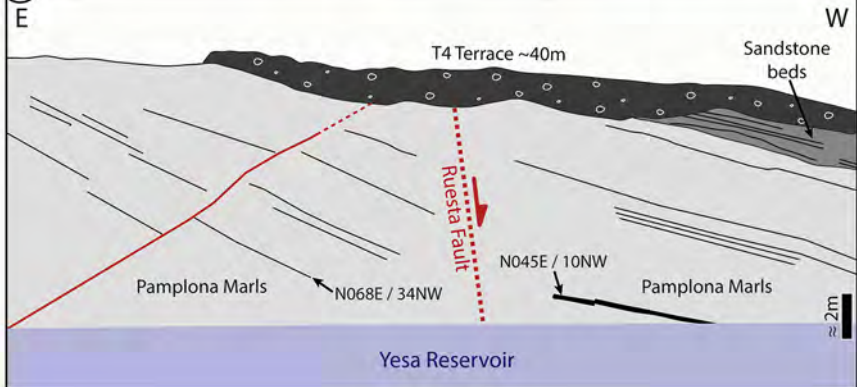
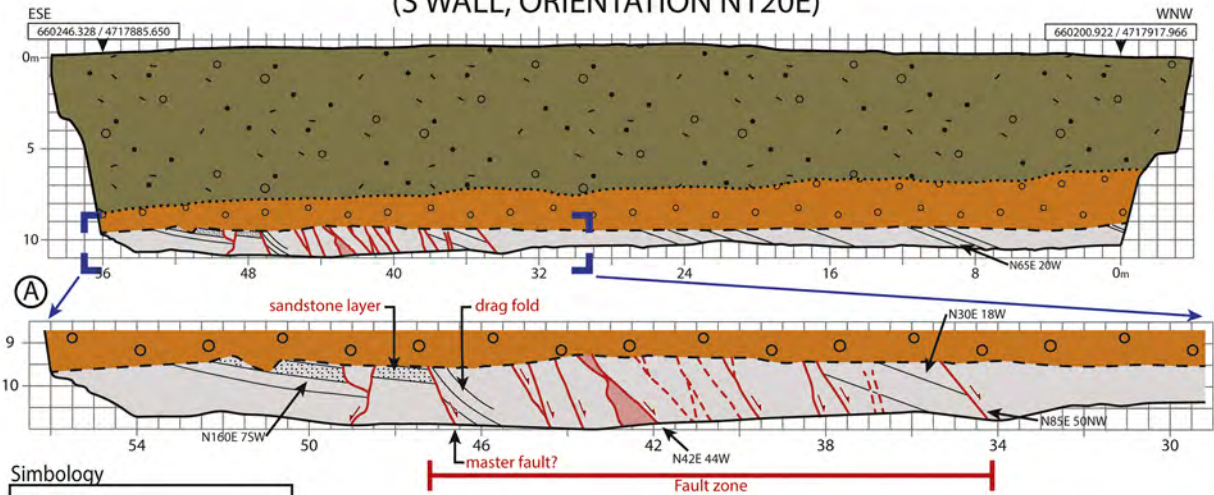


Figure 11

RUESTA FAULT (S WALL, ORIENTATION N120E)



Symbology

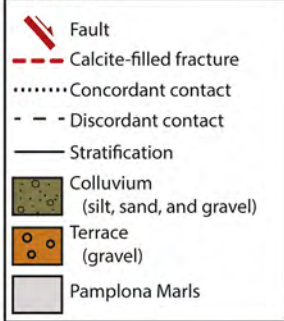


Figure 12